

## Space corner smoothing of CNC machine tools through developing 3D general clothoid

Qun-Bao Xiao<sup>a,b</sup>, Min Wan<sup>\*,a,b</sup>, Yang Liu<sup>a,b</sup>, Xue-Bin Qin<sup>a,b</sup>, Wei-Hong Zhang<sup>a,b,\*</sup>

<sup>a</sup> School of Mechanical Engineering, Northwestern Polytechnical University, Xi'an, Shaanxi 710072, China

<sup>b</sup> State IJR Center of Aerospace Design and Additive Manufacturing, Northwestern Polytechnical University, Xian, Shaanxi 710072, China



### ARTICLE INFO

#### Keywords:

3D clothoid  
Corner smoothing  
 $G^3$  continuity  
G02/G03 commands

### ABSTRACT

Tool paths defined by G01/G02/G03 commands need to be smoothed to eliminate the discontinuities of velocity, acceleration and jerk at the junction points. Because of inherent problems of curve fillets, traditional corner smoothing strategies are limited to the smoothing of corners in plane. This article presents a method to smooth the space corners through blending the position, tangent, curvature and sharpness of the adjacent trajectory segments based on 3D general clothoid splines, which are analytically developed by proposing 3D clothoid with  $G^3$  continuity. The 3D general clothoid realizes extending the traditional clothoid from 2-dimension to 3-dimension, and reserves some good properties of the traditional clothoid, i.e. the curve length parameterization and the analytically expressed curvature. It can also achieve higher degree of continuity compared to the traditional 2D clothoid. Based on the proposed 3D general clothoid, a corner smoothing algorithm, which is suitable for the smoothing of any planar or space line-line, line-arc or arc-arc pairs with  $G^3$  continuity, is proposed. At the same time, a smoothing-error-constraining-algorithm is developed to constrain the smoothing error within the tolerance. Simulation and experimental results, which are obtained from the smoothing of trajectories containing space corners, trajectories containing planar corners with G02/G03 commands, and trajectories containing planar corners with only G01 commands, demonstrate that the proposed corner smoothing algorithm can effectively increase the machining quality and efficiency.

### 1. Introduction

CNC machine tools are widely used to manufacture metallic and composite materials [1–4] by following user-input tool paths. Although tool paths defined by splines are capable of providing smoother and faster motion [5–7], most CNC machine tools are unable to efficiently interpolate parametric splines due to the difficulties in planning time-optimal feed profiles [8,9] and online parametric interpolation [10]. Traditional tool paths are composed of a series of line segments and arcs, known as G01 and G02/G03 commands, which bring about serious discontinuities of velocity, acceleration and jerk at the junction points. These discontinuities cause fierce machine tool vibrations and poor surface finish. To keep the acceleration and jerk within machine tool limits, the NC systems have to slow down and even fully stop the servo axes around corners, which greatly restricts the productivity.

To handle this problem, researchers blend the adjacent line segments or arcs with tiny local curves [11] to achieve velocity, acceleration and jerk continuity, namely local corner smoothing. Erkorkmaz et al. [12] proposed two corner smoothing strategies for 3-axis tool

path, i.e. the under-corner approach and the over-corner approach. Quintic splines were adopted to handle the conditions of under-cut and over-cut. Fan et al. [13] proposed a real-time local corner smoothing algorithm with quadratic Bezier curves. Bi et al. [14] developed an analytical five-axis path-smoothing algorithm with curvature continuous dual-Beizer curves. Li et al. [15] developed a trajectory smoothing method based on reinforcement learning. More corner smoothing algorithms were developed based on B-splines [16–19], PH curves [20,21], kinematic methods [22] and FIR filters [23–25]. To handle the conditions where the line segments are short and massive, global corner smoothing methods were also developed. The short line segments were usually approximated by parametric curves, such as polynomials [26,27], quintic splines [28,29] and B-splines [30,31].

However, all the above works are focused on tool paths composed of only G01 commands. It means that the above methods can only be applied to the smoothing of tool paths composed of a series of line segments. For tool paths containing circular segments (G02/G03 commands), these methods will fail. To solve this problem, researchers resorted to clothoid, which has simple and closed form expressions of

\* Corresponding authors at: School of Mechanical Engineering, Northwestern Polytechnical University, Xi'an, Shaanxi 710072, China.

E-mail addresses: [m.wan@nwpu.edu.cn](mailto:m.wan@nwpu.edu.cn) (M. Wan), [zhangwh@nwpu.edu.cn](mailto:zhangwh@nwpu.edu.cn) (W.-H. Zhang).

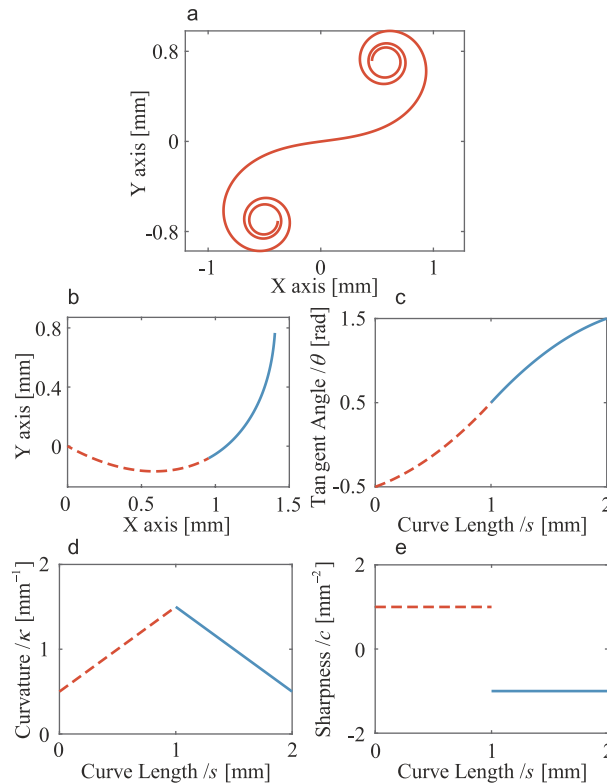


**Fig. 1.** A typical clothoid (a). A two-segment clothoid spline (b) and its tangent angle (c), curvature (d) and sharpness (e).

tangent angle and curvature, and thus is capable of blending line-arc and arc-arc couples. At the same time, because clothoid is curve-length parameterized, trajectories smoothed with clothoid splines are simple and robust in interpolation without feed fluctuation effect [32]. A typical clothoid and a two-segment clothoid spline are shown in Fig. 1(a) and (b), respectively. Jouaneh et al. [33,34] first used two-segment clothoid splines to achieve a curvature continuous transition. Shin and Singh [35] used three-segment clothoid splines to connect every two successive points with tangent and curvature continuity for path planning of robot vehicles. Brezak and Petrović [36] proposed a path smoothing algorithm for differential drive mobile robots. Two-segment clothoid splines are used to smooth the line-line pairs and line-arc pairs with  $G^2$  continuity. Shahzadeh et al. [37] developed a path smoothing algorithm based on clothoid splines with constrained smoothing error for symmetrical conditions. Later, Shahzadeh et al. [38] developed a

corner smoothing algorithm for general line-line pairs, line-arc pairs and arc-arc pairs with two-segment clothoid splines.

The above methods realize the corner smoothing of tool paths containing G0/G03 commands, but have two main shortcomings:

- (1) The above methods are limited to the corner smoothing of trajectories containing only planner corners.
- (2) The above methods are  $G^3$  discontinuous.

Here, planar corners refer to the corners that can be transformed to the X-Y plane through rotation and translation, while space corners refer to the corners that cannot be transformed to the X-Y plane through rotation and translation. These two shortcomings are due to inherent problems of the clothoid, which are illustrated below.

The clothoid can be expressed as follows.

$$\begin{cases} x = x_0 + \int_0^s \cos(\theta_0 + \kappa_0 \tau + \frac{1}{2}c\tau^2)d\tau \\ y = y_0 + \int_0^s \sin(\theta_0 + \kappa_0 \tau + \frac{1}{2}c\tau^2)d\tau \end{cases} \quad (1)$$

where  $x_0$  and  $y_0$  are the starting coordinates of the clothoid.  $s$  is the curve length parameter.  $\theta_0$  and  $\kappa_0$  are the starting tangent angle and curvature.  $c$  is the sharpness, which is the derivative of curvature with respect to curve length, i.e.  $c = dx/ds$ .

Because the clothoid is defined as a planner curve, the clothoid splines can only be planar curves if the continuities of tangent angle and curvature are required. Therefore, the clothoid splines can only achieve the smoothing of planar corners. However, space corners are quite common in the machining process of parts having circular or spherical features. For example, the tool path used to milling a bowl-shape mold contains many corners composed of segments that do not locate in the same plane, as shown in Fig. 2. For this kind of tool paths, the above mentioned corner smoothing strategies [33–38] will fail because the corners cannot be locally transformed to the X-Y plane. It should be noted that there are reports of 3D clothoids [39–41], which are developed from the aesthetic point of view. These 3D clothoids are defined by a group of differential equations and there does not exist analytical expression of their coordinates. This fact makes them inconvenient for the construction of clothoid splines. Thus, it is extremely difficult and even impossible to use these clothoids for the corner smoothing.

The curvature of a traditional two-segment clothoid spline can be expressed as follows.

$$\kappa = \begin{cases} \kappa_0 + c_1 s & 0 \leq s < s_1 \\ \kappa_0 + c_1 s_1 + c_2(s - s_1) & s_1 \leq s \leq s_2 \end{cases} \quad (2)$$

where  $s_1$  and  $s_2$  are the curve length of the two segments of clothoids.  $c_1$

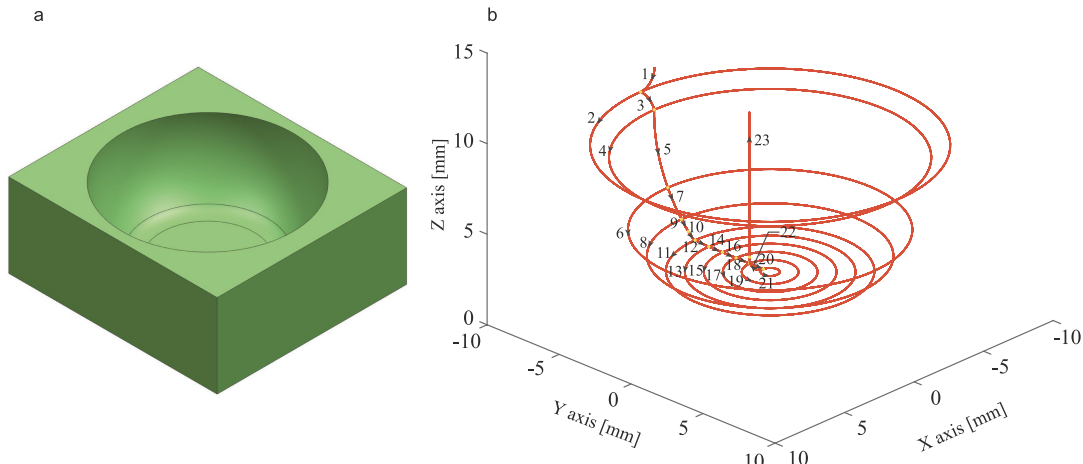


**Fig. 2.** A bowl-shape mold (a) and its milling tool path (b).

and  $c_2$  are the sharpness of the two segments of clothoids. It can be seen from Eq. (2) and Fig. 1(d) that the curvature is linearly related to the curve length  $s$ . Therefore, its derivative, which is the sharpness, is a constant for each segment of clothoid, as can be seen in Eq. (3) and Fig. 1 (e).

$$c = \begin{cases} c_1 & 0 \leq s < s_1 \\ c_2 & s_1 \leq s \leq s_2 \end{cases} \quad (3)$$

Because  $c_1$  and  $c_2$  are different (or the two-segment clothoid spline will become a single segment of clothoid), there is a sharpness jump at the junction point of the two segments, as can be seen from Fig. 1(e). Therefore, the traditional clothoid spline can only achieve  $G^2$  continuity. In conclusion, these two shortcomings are inherent problems of the traditional clothoid. To solve the above two problems, it is needed to make new derivation to develop a 3D clothoid.

This article establishes a thoroughly new method to smooth the trajectories involving space corners in 3-axis CNC machining. The clothoid is extended from 2D to 3D through adding a Z component and keeping the norm of derivative being 1, which is the premise of arc-length parameterization. At the same time, the order of the clothoid is increased by turning the constant sharpness to a function with respect to the curve length. By doing this, the 3D corner smoothing with  $G^3$  continuity is realized. The proposed method can deal with two situations. The first situation is the corner smoothing of line segments (G01 commands) in space, which does not possess extra difficulties since 3D line segments can be treated as 2D corners after locally transforming the adjacent 3D line segments into a plane. The second situation deals with the corner smoothing of line segments and circular segments (G02/G03 commands), and this situation is the focus of this article. As far as the authors' knowledge, it is the first time that 3D corners formed by line segments and arcs or arcs and arcs are smoothed. The  $G^3$  continuity is achieved for the whole smoothed trajectories. At the same time, the errors induced by smoothing are strictly constrained within the tolerance. The rest of this article is organized as follows. Section 2 details the constructing procedure of the 3D general clothoid spline. Section 3 develops an algorithm to smooth 3D corners containing planar or space line-line pairs, line-arc pairs or arc-arc pairs, together with a procedure to constrain the smoothing errors. Simulation and experimental verifications are conducted in Section 4. Finally, conclusions are drawn in Section 5.

## 2. Development of 3D general clothoid spline

In this section, the traditional clothoid is briefly introduced first, and then, the 3D general clothoid is proposed. Finally, based on the proposed curve, the clothoid spline with four segments is developed to smooth the corner.

### 2.1. Introduction of the traditional clothoid

The traditional clothoid is defined that its curvature is a linear function of its curve length.

$$\kappa(s) = \kappa_0 + cs \quad (4)$$

Because the curvature is the derivative of tangent angle with respect to the curve length, the tangent angle can be obtained by integrating the curvature.

$$\theta(s) = \theta_0 + \int_0^s \kappa(s) ds = \theta_0 + \kappa_0 s + \frac{1}{2}cs^2 \quad (5)$$

The unit tangent vector  $\mathbf{T}(s)$  can be calculated as follows.

$$\mathbf{T}(s) = \begin{bmatrix} \cos \theta(s) \\ \sin \theta(s) \end{bmatrix} \quad (6)$$

Because the unit tangent vector is the derivative of the coordinate of the curve ( $\mathbf{P} = [x, y]^T$ ) with respect to the curve length  $s$ , the coordinate of the clothoid can be calculated by integrating the unit tangent vector.

$$\mathbf{T}(s) = \frac{d\mathbf{P}(s)}{ds} \Rightarrow \mathbf{P}(s) = \mathbf{P}_0 + \int_0^s \mathbf{T}(\tau) d\tau \quad (7)$$

Substituting Eqs. (5) and (6) into Eq. (7) leads to the coordinate of clothoid.

$$\begin{aligned} x(s) &= x_0 + \int_0^s \cos(\theta_0 + \kappa_0 \tau + \frac{1}{2}c\tau^2) d\tau \\ y(s) &= y_0 + \int_0^s \sin(\theta_0 + \kappa_0 \tau + \frac{1}{2}c\tau^2) d\tau \end{aligned} \quad (8)$$

### 2.2. Development of 3D general clothoid

The traditional clothoid cannot be applied to the smoothing of 3D corners, and cannot achieve  $G^3$  continuity. The 3D general clothoid that can remedy these two drawbacks is proposed as follows.

$$\begin{aligned} x(u) &= x_0 + \int_0^u \cos(\theta_1(\tau)) \cos(\theta_2(\tau)) d\tau \\ y(u) &= y_0 + \int_0^u \cos(\theta_1(\tau)) \sin(\theta_2(\tau)) d\tau \\ z(u) &= z_0 + \int_0^u \sin(\theta_1(\tau)) d\tau \end{aligned} \quad (9)$$

with

$$\begin{aligned} \theta_1(u) &= \sum_{k=0}^n \frac{a_{1,k}}{k!} u^k \\ \theta_2(u) &= \sum_{k=0}^n \frac{a_{2,k}}{k!} u^k \end{aligned} \quad (10)$$

where  $x_0, y_0, z_0$  are the starting coordinates of the 3D general clothoid.  $a_{1,k}$  and  $a_{2,k}$  ( $k = 0, 1, \dots, n$ ) are the coefficients of  $\theta_1(s)$  and  $\theta_2(s)$ .  $n$  is the order of the 3D general clothoid curve.

**Theorem 1.** The curve parameter  $u$  of the 3D general clothoid is just the curve length  $s$ .

**Proof.** The tangent vector of the 3D general clothoid is

$$\mathbf{T}(u) = \mathbf{P}'(u) = \begin{bmatrix} x'(u) \\ y'(u) \\ z'(u) \end{bmatrix} = \begin{bmatrix} \cos(\theta_1(u)) \cos(\theta_2(u)) \\ \cos(\theta_1(u)) \sin(\theta_2(u)) \\ \sin(\theta_1(u)) \end{bmatrix} \quad (11)$$

The curve length  $s$  of the 3D general clothoid can be calculated as follows.

$$\begin{aligned} s &= \int_0^u \|\mathbf{T}(\tau)\|_2 d\tau = \int_0^u \sqrt{(x'(\tau))^2 + (y'(\tau))^2 + (z'(\tau))^2} d\tau = \int_0^u 1 d\tau \\ &= u \end{aligned} \quad (12)$$

where  $\|\cdot\|_2$  means the 2-norm.

The theorem is proved.  $\square$

**Theorem 2.** The  $n$ th order 3D general clothoid can achieve the corner smoothing with  $G^n$  continuity.

**Proof.** The  $(n-1)$ th order derivatives of  $\theta_1$  and  $\theta_2$  with respect to  $s$  are

$$\begin{aligned} \theta_1^{(n-1)}(s) &= a_{1,n-1} + a_{1,n}s \\ \theta_2^{(n-1)}(s) &= a_{2,n-1} + a_{2,n}s \end{aligned} \quad (13)$$

which are linear functions of curve length  $s$ . Therefore, 3D general clothoid splines with continuous  $(n-1)$ th order derivatives of  $\theta_1(s)$  and  $\theta_2(s)$  can be constructed. Because  $\theta_1(s)$  and  $\theta_2(s)$  are  $(n-1)$ th order continuous,  $\cos(\theta_1(s))$ ,  $\sin(\theta_1(s))$ ,  $\cos(\theta_2(s))$  and  $\sin(\theta_2(s))$  are  $(n-1)$ th order continuous. Therefore, the derivatives of  $x$ ,  $y$ ,  $z$  coordinates of the 3D general clothoid splines (i.e. Eq. (11)) are  $(n-1)$ th order continuous. Hence, the 3D general clothoid splines

are the  $n$ th order continuous. The theorem is proved.  $\square$

The third-order 3D general clothoid can be written as follows.

$$\begin{aligned} x(s) &= x_0 + \int_0^s \cos(\theta_{1,0} + \kappa_{1,0}\tau + \frac{1}{2}c_{1,0}\tau^2 + \frac{1}{6}\gamma_1\tau^3)\cos(\theta_{2,0} \\ &\quad + \kappa_{2,0}\tau + \frac{1}{2}c_{2,0}\tau^2 + \frac{1}{6}\gamma_2\tau^3)d\tau \\ y(s) &= y_0 + \int_0^s \cos(\theta_{1,0} + \kappa_{1,0}\tau + \frac{1}{2}c_{1,0}\tau^2 + \frac{1}{6}\gamma_1\tau^3)\sin(\theta_{2,0} \\ &\quad + \kappa_{2,0}\tau + \frac{1}{2}c_{2,0}\tau^2 + \frac{1}{6}\gamma_2\tau^3)d\tau \\ z(s) &= z_0 + \int_0^s \sin(\theta_{1,0} + \kappa_{1,0}\tau + \frac{1}{2}c_{1,0}\tau^2 + \frac{1}{6}\gamma_1\tau^3)d\tau \end{aligned} \quad (14)$$

where  $\theta_{1,0}$ ,  $\theta_{2,0}$ ,  $\kappa_{1,0}$ ,  $\kappa_{2,0}$ ,  $c_{1,0}$ ,  $c_{2,0}$ ,  $\gamma_1$  and  $\gamma_2$  are parameters of the 3D general clothoid. It can be seen that the traditional clothoid is a special case of the 3D general clothoid with  $\theta_{1,0} = \kappa_{1,0} = c_{1,0} = \gamma_1 = \gamma_2 = 0$ .

**Property 1.** The curvature of the 3D general clothoid can be analytically calculated, which is  $\kappa(s) = \sqrt{\theta'_1(s)^2 + \cos^2(\theta_1(s))\theta'_2(s)^2}$ .

**Proof.** According to the first derivative of the 3D general clothoid (i.e. Eq. (11)), the second derivative with respect to the curve length  $s$  can be calculated as follows.

$$\mathbf{P}''(s) = \begin{bmatrix} x''(s) \\ y''(s) \\ z''(s) \end{bmatrix} = \begin{bmatrix} -\sin(\theta_1(s))\cos(\theta_2(s))\theta'_1(s) - \cos(\theta_1(s))\sin(\theta_2(s))\theta'_2(s) \\ -\sin(\theta_1(s))\sin(\theta_2(s))\theta'_1(s) + \cos(\theta_1(s))\cos(\theta_2(s))\theta'_2(s) \\ \cos(\theta_1(s))\theta'_1(s) \end{bmatrix} \quad (15)$$

Next, the curvature can be calculated.

$$\begin{aligned} \kappa(s) &= \|\mathbf{P}''(s)\|_2 = \sqrt{x''(s)^2 + y''(s)^2 + z''(s)^2} \\ &= \sqrt{\theta'_1(s)^2 + \cos^2(\theta_1(s))\theta'_2(s)^2} \end{aligned} \quad (16)$$

The property is proved.  $\square$

It can be seen that the 3D general clothoid is defined as a space curve, which makes it possible to smooth space corners. At the same time, it can achieve  $G^3$  continuity according to Theorem 2, and reserves some good properties of the traditional clothoid, i.e. curve length parameterization and analytically expressed curvature.

### 2.3. Formulation of 3D general clothoid spline

Based on the proposed 3D general clothoid, a four-segment 3D general clothoid spline for corner smoothing is developed in this section. The four-segment 3D general clothoid spline can be expressed as follows.

$$\gamma_i(s) = \theta_i''(s) = \begin{cases} \gamma_{i,1} & 0 \leq s \leq \bar{s}_1 \\ \gamma_{i,2} & \bar{s}_1 < s \leq \bar{s}_2 \\ \gamma_{i,3} & \bar{s}_2 < s \leq \bar{s}_3 \\ \gamma_{i,4} & \bar{s}_3 < s \leq \bar{s}_4 \end{cases} \quad (17)$$

$$c_i(s) = \theta_i''(s) = \begin{cases} c_{i,0} + \gamma_{i,1}s & 0 \leq s \leq \bar{s}_1 \\ c_{i,1} + \gamma_{i,2}(s - \bar{s}_1) & \bar{s}_1 < s \leq \bar{s}_2 \\ c_{i,2} + \gamma_{i,3}(s - \bar{s}_2) & \bar{s}_2 < s \leq \bar{s}_3 \\ c_{i,3} + \gamma_{i,4}(s - \bar{s}_3) & \bar{s}_3 < s \leq \bar{s}_4 \end{cases} \quad (18)$$

$$\kappa_i(s) = \theta_i'(s) = \begin{cases} \kappa_{i,0} + c_{i,0}s + \frac{1}{2}\gamma_{i,1}s^2 & 0 \leq s \leq \bar{s}_1 \\ \kappa_{i,1} + c_{i,1}(s - \bar{s}_1) + \frac{1}{2}\gamma_{i,2}(s - \bar{s}_1)^2 & \bar{s}_1 < s \leq \bar{s}_2 \\ \kappa_{i,2} + c_{i,2}(s - \bar{s}_2) + \frac{1}{2}\gamma_{i,3}(s - \bar{s}_2)^2 & \bar{s}_2 < s \leq \bar{s}_3 \\ \kappa_{i,3} + c_{i,3}(s - \bar{s}_3) + \frac{1}{2}\gamma_{i,4}(s - \bar{s}_3)^2 & \bar{s}_3 < s \leq \bar{s}_4 \end{cases} \quad (19)$$

$$\theta_i(s) = \begin{cases} \theta_{i,0} + \kappa_{i,0}s + \frac{1}{2}c_{i,0}s^2 + \frac{1}{6}\gamma_{i,1}s^3 & 0 \leq s \leq \bar{s}_1 \\ \theta_{i,1} + \kappa_{i,1}(s - \bar{s}_1) + \frac{1}{2}c_{i,1}(s - \bar{s}_1)^2 + \frac{1}{6}\gamma_{i,2}(s - \bar{s}_1)^3 & \bar{s}_1 < s \leq \bar{s}_2 \\ \theta_{i,2} + \kappa_{i,2}(s - \bar{s}_2) + \frac{1}{2}c_{i,2}(s - \bar{s}_2)^2 + \frac{1}{6}\gamma_{i,3}(s - \bar{s}_2)^3 & \bar{s}_2 < s \leq \bar{s}_3 \\ \theta_{i,3} + \kappa_{i,3}(s - \bar{s}_3) + \frac{1}{2}c_{i,3}(s - \bar{s}_3)^2 + \frac{1}{6}\gamma_{i,4}(s - \bar{s}_3)^3 & \bar{s}_3 < s \leq \bar{s}_4 \end{cases} \quad (20)$$

with

$$\begin{cases} c_{i,1} = c_{i,0} + \gamma_{i,1}\bar{s}_1 \\ c_{i,2} = c_{i,1} + \gamma_{i,2}\bar{s}_2 \\ c_{i,3} = c_{i,2} + \gamma_{i,3}\bar{s}_3 \\ c_{i,4} = c_{i,3} + \gamma_{i,4}\bar{s}_4 \end{cases} \quad (21)$$

$$\begin{cases} \kappa_{i,1} = \kappa_{i,0} + c_{i,0}\bar{s}_1 + \frac{1}{2}\gamma_{i,1}\bar{s}_1^2 \\ \kappa_{i,2} = \kappa_{i,1} + c_{i,1}\bar{s}_2 + \frac{1}{2}\gamma_{i,2}\bar{s}_2^2 \\ \kappa_{i,3} = \kappa_{i,2} + c_{i,2}\bar{s}_3 + \frac{1}{2}\gamma_{i,3}\bar{s}_3^2 \\ \kappa_{i,4} = \kappa_{i,3} + c_{i,3}\bar{s}_4 + \frac{1}{2}\gamma_{i,4}\bar{s}_4^2 \end{cases} \quad (22)$$

$$\begin{cases} \theta_{i,1} = \theta_{i,0} + \kappa_{i,0}\bar{s}_1 + \frac{1}{2}c_{i,0}\bar{s}_1^2 + \frac{1}{6}\gamma_{i,1}\bar{s}_1^3 \\ \theta_{i,2} = \theta_{i,1} + \kappa_{i,1}\bar{s}_2 + \frac{1}{2}c_{i,1}\bar{s}_2^2 + \frac{1}{6}\gamma_{i,2}\bar{s}_2^3 \\ \theta_{i,3} = \theta_{i,2} + \kappa_{i,2}\bar{s}_3 + \frac{1}{2}c_{i,2}\bar{s}_3^2 + \frac{1}{6}\gamma_{i,3}\bar{s}_3^3 \\ \theta_{i,4} = \theta_{i,3} + \kappa_{i,3}\bar{s}_4 + \frac{1}{2}c_{i,3}\bar{s}_4^2 + \frac{1}{6}\gamma_{i,4}\bar{s}_4^3 \end{cases} \quad (23)$$

where  $i = 1, 2$ .  $\bar{s}_1 = s_1$ ,  $\bar{s}_2 = s_1 + s_2$ ,  $\bar{s}_3 = s_1 + s_2 + s_3$  and  $\bar{s}_4 = s_1 + s_2 + s_3 + s_4$ .  $s_1$ ,  $s_2$ ,  $s_3$  and  $s_4$  are the curve length of the four segments of clothoids.  $\theta_{i,j}$ ,  $\kappa_{i,j}$ ,  $c_{i,j}$ ,  $\gamma_{i,j}$  ( $i = 1, 2$ ;  $j = 0, 1, 2, 3, 4$ ) are the parameters related to the  $j$ th knot. It can be seen from Eqs. (17)-(20) that  $\theta_i$ ,  $\kappa_i$ ,  $c_i$  ( $i = 1, 2$ ) are continuous at the junction points.

$$\begin{cases} \theta_i(\bar{s}_j - 0) = \theta_i(\bar{s}_j + 0) \\ \kappa_i(\bar{s}_j - 0) = \kappa_i(\bar{s}_j + 0) & i = 1, 2; j = 1, 2, 3 \\ c_i(\bar{s}_j - 0) = c_i(\bar{s}_j + 0) \end{cases} \quad (24)$$

where  $f(\bar{s}_j - 0) = \lim_{\varepsilon \rightarrow 0^+} f(\bar{s}_j - \varepsilon)$ ,  $f(\bar{s}_j + 0) = \lim_{\varepsilon \rightarrow 0^+} f(\bar{s}_j + \varepsilon)$ . Because  $\theta_i$ ,  $\kappa_i$  and  $c_i$  ( $i = 1, 2$ ) are continuous, the general clothoid spline is  $G^3$  continuous. A typical four-segment 3D general clothoid spline is shown in Fig. 3(a). Its tangent vector, curvature, sharpness and torsion are shown in Fig. 3(b)-(e), respectively. It can be seen that its curvature is smooth. Its sharpness is continuous, which indicates that it is  $G^3$  continuous. Its torsion is nonzero, which indicates that it is a space curve.

### 3. Smoothing of space corners

#### 3.1. Fitting of tool paths in 3D space

In this section, the corner smoothing algorithm is developed based on the proposed 3D general clothoid spline. Because the clothoid is defined with respect to the Fresnel integral, which cannot be calculated analytically, the proposed corner smoothing algorithm is carried out in the off-line pre-processor, as shown in Fig. 4.

The space straight lines (G01 commands) can be represented as follows.

$$\mathbf{P}_{\text{traj}}(s) = \mathbf{P}_{l0} + \mathbf{v}_ls \quad (25)$$

where  $\mathbf{P}_{\text{traj}}(s) = [x_{\text{traj}}(s), y_{\text{traj}}(s), z_{\text{traj}}(s)]^T$  is a trajectory point.

$\mathbf{v}_l = \frac{\mathbf{P}_{le} - \mathbf{P}_{l0}}{\|\mathbf{P}_{le} - \mathbf{P}_{l0}\|_2}$  is the unit direction vector of the line segment, as shown in Fig. 5(a).  $\mathbf{P}_{l0}$  and  $\mathbf{P}_{le}$  are the start and end points of the line segment. The derivatives of the straight line can be represented as follows.

$$\begin{aligned} \mathbf{P}'_{\text{traj}}(s) &= \mathbf{v}_l \\ \mathbf{P}''_{\text{traj}}(s) &= \mathbf{P}''_{\text{traj}}(s) = [0, 0, 0]^T \end{aligned} \quad (26)$$

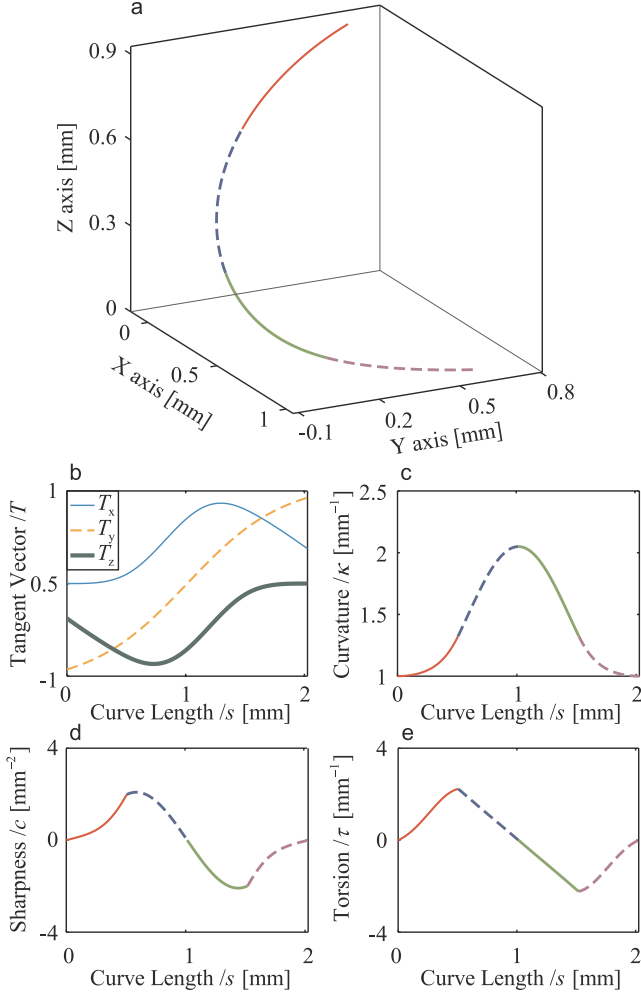


**Fig. 3.** A typical four-segment clothoid spline (a) and its tangent vector (b), curvature (c), sharpness (d) and torsion (e).

where

$$\mathbf{P}'_{\text{traj}}(s) = [x'_{\text{traj}}(s), y'_{\text{traj}}(s), z'_{\text{traj}}(s)]^T, \mathbf{P}''_{\text{traj}}(s)$$

$$= [x''_{\text{traj}}(s), y''_{\text{traj}}(s), z''_{\text{traj}}(s)]^T, \mathbf{P}'''_{\text{traj}}(s) = [x'''_{\text{traj}}(s), y'''_{\text{traj}}(s), z'''_{\text{traj}}(s)]^T$$

the first, the second and the third derivatives of the line segment.

The space arcs (G02/G03) can be represented as follows.

$$\mathbf{P}_{\text{traj}}(\varphi) = \mathbf{P}_c + r \cos(\varphi) \mathbf{v}_{a1} + r \sin(\varphi) \mathbf{v}_{a2} \quad (27)$$

where  $\mathbf{v}_{a1} = \frac{\mathbf{P}_{a0} - \mathbf{P}_c}{\|\mathbf{P}_{a0} - \mathbf{P}_c\|_2}$  is the unit vector from the center ( $\mathbf{P}_c$ ) to the start point ( $\mathbf{P}_{a0}$ ) of the arc, as shown in Fig. 5(b).  $\mathbf{v}_{a2}$  is the unit vector that lies in the plane of the space arc and is perpendicular to  $\mathbf{v}_{a1}$ .  $\varphi$  is the angle between the vectors  $\overrightarrow{\mathbf{P}_c \mathbf{P}_{\text{traj}}}$  and  $\mathbf{v}_{a1}$ .

Because the curve length from the start point  $\mathbf{P}_{a0}$  to  $\mathbf{P}_{\text{traj}}$  can be represented as  $s = r\varphi$ ,  $\varphi$  can be solved as follows.

$$\varphi = \frac{s}{r} \quad (28)$$

Substitute Eq. (28) into Eq. (27), the arc trajectory can be expressed as a function with respect to the curve length  $s$ .

$$\mathbf{P}_{\text{traj}}(s) = \mathbf{P}_c + r \cos\left(\frac{s}{r}\right) \mathbf{v}_{a1} + r \sin\left(\frac{s}{r}\right) \mathbf{v}_{a2} \quad (29)$$

Based on the expression of space arcs (i.e. Eq. (29)), the derivatives of the trajectory with respect to the curve length  $s$  can be calculated as follows.

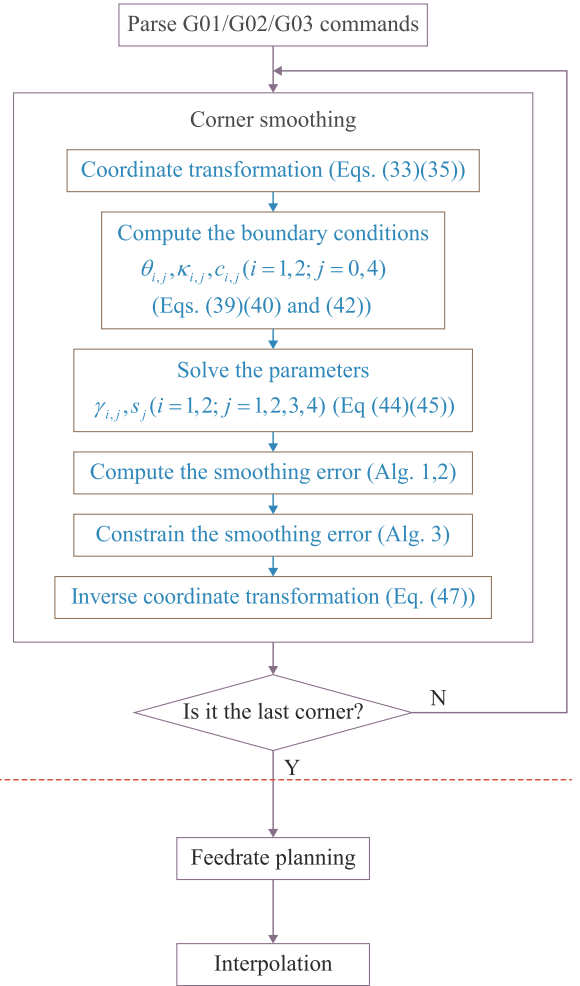


**Fig. 4.** The flow chart of the corner smoothing algorithm.

$$\begin{aligned} \mathbf{P}'_{\text{traj}}(s) &= -\sin\left(\frac{s}{r}\right) \mathbf{v}_{a1} + \cos\left(\frac{s}{r}\right) \mathbf{v}_{a2} \\ \mathbf{P}''_{\text{traj}}(s) &= -\frac{1}{r} \cos\left(\frac{s}{r}\right) \mathbf{v}_{a1} - \frac{1}{r} \sin\left(\frac{s}{r}\right) \mathbf{v}_{a2} \\ \mathbf{P}'''_{\text{traj}}(s) &= \frac{1}{r^2} \sin\left(\frac{s}{r}\right) \mathbf{v}_{a1} - \frac{1}{r^2} \cos\left(\frac{s}{r}\right) \mathbf{v}_{a2} \end{aligned} \quad (30)$$

Before blending corners with 3D general clothoid splines, the coordinate transformation is first conducted to coincide the normal direction of the corner with the positive direction of Z-axis, as shown in Fig. 6. The tangent vectors  $\mathbf{v}_1$  and  $\mathbf{v}_2$  of the trajectory around the corner are

$$\begin{aligned} \mathbf{v}_1 &= \mathbf{P}'_{\text{traj},1}(s_c) \\ \mathbf{v}_2 &= \mathbf{P}'_{\text{traj},2}(s_c) \end{aligned} \quad (31)$$

where  $\mathbf{P}'_{\text{traj},1}(s)$  and  $\mathbf{P}'_{\text{traj},2}(s)$  are the derivatives of the first and the second segments of the trajectory with respect to the curve length  $s$ .  $s_c$  is the curve length parameter corresponding to the corner point. The normal vector of the corner, i.e.  $\mathbf{n} = [n_x, n_y, n_z]^T$  in Fig. 6, can be calculated as follows.

$$\mathbf{n} = \begin{cases} \mathbf{v}_1 \times \mathbf{v}_2 & \text{if } \mathbf{v}_1 \# \mathbf{v}_2 \\ \mathbf{n}_1 & \text{if } \mathbf{v}_1 \parallel \mathbf{v}_2 \text{ and } \mathbf{n}_1 \text{ exists} \\ \mathbf{n}_2 & \text{if } \mathbf{v}_1 \parallel \mathbf{v}_2 \text{ and } \mathbf{n}_2 \text{ exists} \end{cases} \quad (32)$$

where “ $\times$ ” means cross product. “ $\parallel$ ” means collinear and “ $\#$ ” means non-collinear.  $\mathbf{n}_1$  and  $\mathbf{n}_2$  are the normal vectors of the first and the second segments of the trajectory.  $\mathbf{n}_1$  and  $\mathbf{n}_2$  exist if the segment of trajectory is an arc. To coincide the normal vector  $\mathbf{n}$  with the positive direction of Z-axis, the transfer matrix can be calculated as follows.

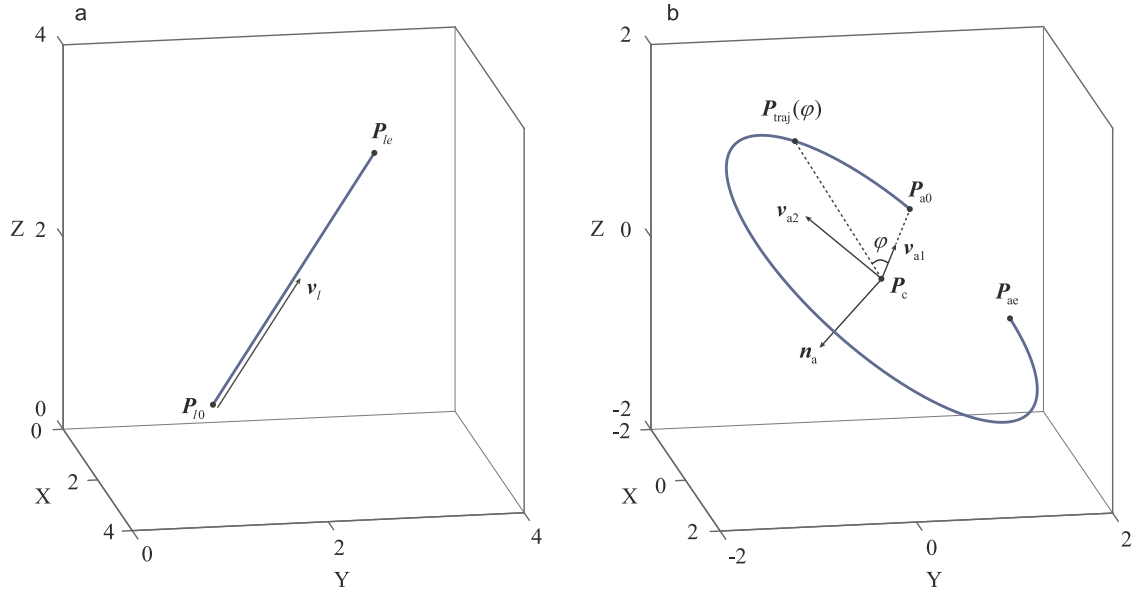


**Fig. 5.** A space line segment (a) and a space arc (b).

$$T = \begin{cases} \begin{bmatrix} w & -\frac{n_x n_y}{w} & -\frac{n_x n_z}{w} \\ 0 & \frac{n_z}{w} & -\frac{n_y}{w} \\ n_x & n_y & n_z \end{bmatrix} & \text{if } w \neq 0 \\ \begin{bmatrix} 0 & 0 & \text{sign}(n_x) \\ 0 & 1 & 0 \\ -\text{sign}(n_x) & 0 & 0 \end{bmatrix} & \text{if } w = 0 \end{cases} \quad (33)$$

where  $w = \sqrt{n_y^2 + n_z^2}$ .  $\text{sign}(\cdot)$  is the sign function with the following definition.

$$\text{sign}(n_x) = \begin{cases} 1 & \text{if } n_x > 0 \\ 0 & \text{if } n_x = 0 \\ -1 & \text{if } n_x < 0 \end{cases} \quad (34)$$

The trajectory points and their derivatives after transformation ( $\tilde{P}_{\text{traj}}(s)$ ,

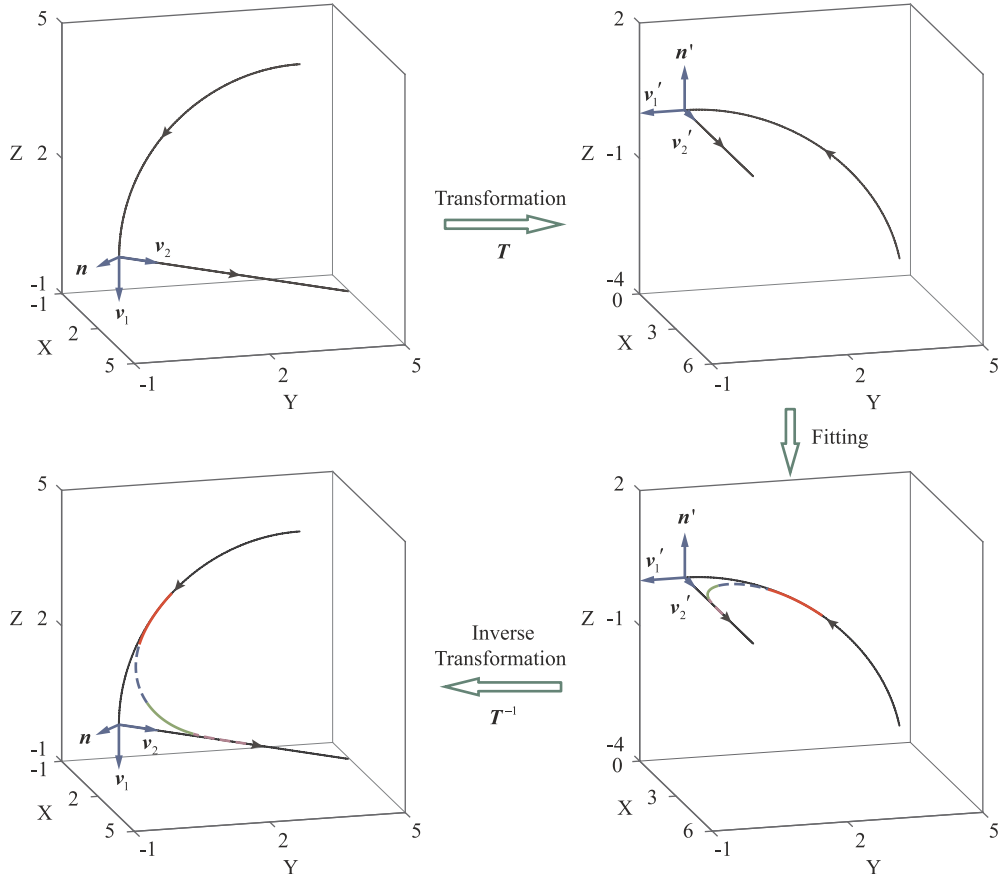


**Fig. 6.** Transformations of the space corners before and after corner smoothing.

$\tilde{\mathbf{P}}'_{\text{traj}}(s)$ ,  $\tilde{\mathbf{P}}'_{\text{traj}}(s)$  and  $\tilde{\mathbf{P}}''_{\text{traj}}(s)$ ) can then be calculated as follows.

$$\begin{cases} \tilde{\mathbf{P}}'_{\text{traj}}(s) = \mathbf{T}\mathbf{P}_{\text{traj}}(s) \\ \tilde{\mathbf{P}}'_{\text{traj}}(s) = \mathbf{T}\mathbf{P}'_{\text{traj}}(s) \\ \tilde{\mathbf{P}}''_{\text{traj}}(s) = \mathbf{T}\mathbf{P}''_{\text{traj}}(s) \\ \tilde{\mathbf{P}}'''_{\text{traj}}(s) = \mathbf{T}\mathbf{P}'''_{\text{traj}}(s) \end{cases} \quad (35)$$

To achieve corner smoothing with  $G^3$  continuity, the derivatives  $\mathbf{P}'(s)$ ,  $\mathbf{P}''(s)$  and  $\mathbf{P}'''(s)$  at the start and the end points of the clothoid spline should equal to those of the original trajectory, i.e. the lines (G01) or arcs (G02/G03).

$$\mathbf{P}'(0) = \tilde{\mathbf{P}}'_{\text{traj}}(s_0), \quad \mathbf{P}'(s_e) = \tilde{\mathbf{P}}'_{\text{traj}}(s_e) \quad (36)$$

$$\mathbf{P}''(0) = \tilde{\mathbf{P}}''_{\text{traj}}(s_0), \quad \mathbf{P}''(s_e) = \tilde{\mathbf{P}}''_{\text{traj}}(s_e) \quad (37)$$

$$\mathbf{P}'''(0) = \tilde{\mathbf{P}}'''_{\text{traj}}(s_0), \quad \mathbf{P}'''(s_e) = \tilde{\mathbf{P}}'''_{\text{traj}}(s_e) \quad (38)$$

where  $s_0$  and  $s_e$  are the curve length parameters of the original trajectory (lines and arcs) at the start and the end points of the clothoid. Substitute Eqs. (11), (20) and (23) into Eq. (36),  $\theta_{i,j}(i=1,2; j=0,4)$  can be solved as follows.

$$\begin{aligned} \theta_{1,0} &= \arcsin(\tilde{z}_{\text{traj}}'(s_0)) \\ \theta_{2,0} &= \begin{cases} \arccos(\frac{\tilde{x}_{\text{traj}}'(s_0)}{\cos(\theta_{1,0})}) & \text{if } \tilde{y}_{\text{traj}}'(s_0) \geq 0 \\ 2\pi - \arccos(\frac{\tilde{x}_{\text{traj}}'(s_0)}{\cos(\theta_{1,0})}) & \text{if } \tilde{y}_{\text{traj}}'(s_0) < 0 \end{cases} \\ \theta_{1,4} &= \arcsin(\tilde{z}_{\text{traj}}'(s_e)) \\ \theta_{2,4} &= \begin{cases} \arccos(\frac{\tilde{x}_{\text{traj}}'(s_e)}{\cos(\theta_{1,4})}) & \text{if } \tilde{y}_{\text{traj}}'(s_e) \geq 0 \\ 2\pi - \arccos(\frac{\tilde{x}_{\text{traj}}'(s_e)}{\cos(\theta_{1,4})}) & \text{if } \tilde{y}_{\text{traj}}'(s_e) < 0 \end{cases} \end{aligned} \quad (39)$$

Substitute Eqs. (15), (19) and (22) into Eq. (37),  $\kappa_{i,j}(i=1,2; j=0,4)$  can be solved as follows.

$$\begin{aligned} \kappa_{1,0} &= \frac{\tilde{z}_{\text{traj}}'(s_0)}{\cos(\theta_{1,0})} \\ \kappa_{2,0} &= \begin{cases} -\frac{\tilde{x}_{\text{traj}}'(s_0) + \sin(\theta_{1,0})\cos(\theta_{2,0})\kappa_{1,0}}{\cos(\theta_{1,0})\sin(\theta_{2,0})} & \text{if } \sin(\theta_{2,0}) \neq 0 \\ \frac{\tilde{x}_{\text{traj}}''(s_0) + \sin(\theta_{1,0})\sin(\theta_{2,0})\kappa_{1,0}}{\cos(\theta_{1,0})\cos(\theta_{2,0})} & \text{if } \sin(\theta_{2,0}) = 0 \end{cases} \\ \kappa_{1,4} &= \frac{\tilde{z}_{\text{traj}}''(s_e)}{\cos(\theta_{1,4})} \\ \kappa_{2,4} &= \begin{cases} -\frac{\tilde{x}_{\text{traj}}''(s_e) + \sin(\theta_{1,4})\cos(\theta_{2,4})\kappa_{1,4}}{\cos(\theta_{1,4})\sin(\theta_{2,4})} & \text{if } \sin(\theta_{2,4}) \neq 0 \\ \frac{\tilde{x}_{\text{traj}}'''(s_e) + \sin(\theta_{1,4})\sin(\theta_{2,4})\kappa_{1,4}}{\cos(\theta_{1,4})\cos(\theta_{2,4})} & \text{if } \sin(\theta_{2,4}) = 0 \end{cases} \end{aligned} \quad (40)$$

The third order derivative of the 3D general clothoid spline can be represented as follows.

$$\begin{aligned} \mathbf{P}'''(s) = & \begin{bmatrix} x'''(s) \\ y'''(s) \\ z'''(s) \end{bmatrix} = \begin{bmatrix} -\cos(\theta_1)\cos(\theta_2)\theta_1'^2 + \sin(\theta_1)\sin(\theta_2)\theta_1'\theta_2' \\ -\cos(\theta_1)\sin(\theta_2)\theta_1'^2 - \sin(\theta_1)\cos(\theta_2)\theta_1'\theta_2' \\ -\sin(\theta_1)\theta_1'^2 \end{bmatrix} \\ & \begin{bmatrix} -\sin(\theta_1)\cos(\theta_2)\theta_1'' + \sin(\theta_1)\sin(\theta_2)\theta_1'\theta_2' - \cos(\theta_1)\cos(\theta_2)\theta_2'^2 - \cos(\theta_1)\sin(\theta_2)\theta_2'' \\ -\sin(\theta_1)\sin(\theta_2)\theta_1'' - \sin(\theta_1)\cos(\theta_2)\theta_1'\theta_2' - \cos(\theta_1)\sin(\theta_2)\theta_2'^2 + \cos(\theta_1)\cos(\theta_2)\theta_2'' \\ +\cos(\theta_1)\theta_1'' \end{bmatrix} \end{aligned} \quad (41)$$

where  $\theta_i$ ,  $\theta'_i$  and  $\theta''_i$  are short for  $\theta_i(s)$ ,  $\theta'_i(s)$  and  $\theta''_i(s)$  ( $i = 1, 2$ ). Substitute Eqs. (18), (21) and (41) into Eq. (38),  $c_{i,j}(i = 1, 2; j = 0, 4)$  can be solved as follows.

$$\begin{aligned} c_{1,0} &= \frac{\tilde{z}_{\text{traj}}''(s_0) + \sin(\theta_{1,0})\kappa_{1,0}^2}{\cos(\theta_{1,0})} \\ c_{2,0} &= \begin{cases} -\frac{\tilde{x}_{\text{traj}}''(s_0) + M_0}{\cos(\theta_{1,0})\sin(\theta_{2,0})} & \text{if } \sin(\theta_{2,0}) \neq 0 \\ \frac{\tilde{y}_{\text{traj}}''(s_0) + N_0}{\cos(\theta_{1,0})\cos(\theta_{2,0})} & \text{if } \sin(\theta_{2,0}) = 0 \end{cases} \\ c_{1,4} &= \frac{\tilde{z}_{\text{traj}}''(s_e) + \sin(\theta_{1,4})\kappa_{1,4}^2}{\cos(\theta_{1,4})} \\ c_{2,4} &= \begin{cases} -\frac{\tilde{x}_{\text{traj}}''(s_e) + M_4}{\cos(\theta_{1,4})\sin(\theta_{2,4})} & \text{if } \sin(\theta_{2,4}) \neq 0 \\ \frac{\tilde{y}_{\text{traj}}''(s_e) + N_4}{\cos(\theta_{1,4})\cos(\theta_{2,4})} & \text{if } \sin(\theta_{2,4}) = 0 \end{cases} \end{aligned} \quad (42)$$

with

$$\begin{aligned} M_j &= \cos(\theta_{1,j})\cos(\theta_{2,j})\kappa_{1,j}^2 - \sin(\theta_{1,j})\sin(\theta_{2,j})\kappa_{1,j}\kappa_{2,j} + \sin(\theta_{1,j})\cos(\theta_{2,i})c_{1,j} \\ &\quad - \sin(\theta_{1,j})\sin(\theta_{2,j})\kappa_{1,j}\kappa_{2,j} + \cos(\theta_{1,j})\cos(\theta_{2,j})\kappa_{2,j}^2 \\ N_j &= \cos(\theta_{1,j})\sin(\theta_{2,j})\kappa_{1,j}^2 + \sin(\theta_{1,j})\cos(\theta_{2,j})\kappa_{1,j}\kappa_{2,j} + \sin(\theta_{1,j})\sin(\theta_{2,i})c_{1,j} \\ &\quad + \sin(\theta_{1,j})\cos(\theta_{2,j})\kappa_{1,j}\kappa_{2,j} + \cos(\theta_{1,j})\sin(\theta_{2,j})\kappa_{2,j}^2 \end{aligned} \quad (43)$$

The boundary parameters  $\theta_{i,j}$ ,  $\kappa_{i,j}$  and  $c_{i,j}(i = 1, 2; j = 0, 4)$  of the clothoid spline have all been solved.

Next, the parameters  $\gamma_{i,j}$  and  $s_j(i = 1, 2; j = 1, 2, 3, 4)$  of the clothoid spline are to be solved. According to Eqs. (9), (21), (22) and (23), the following equations can be obtained.

$$\left. \begin{array}{l} G^3 \text{ continuity: } c_{i,0} + \sum_{h=1}^4 \gamma_{i,h} s_h = c_{i,4} \\ G^2 \text{ continuity: } \kappa_{i,0} + \sum_{h=1}^4 \left( c_{i,h-1} s_h + \frac{1}{2} \gamma_{i,h} s_h^2 \right) = \kappa_{i,4} \\ G^1 \text{ continuity: } \theta_{i,0} + \sum_{h=1}^4 \left( \kappa_{i,h-1} s_h + \frac{1}{2} c_{i,h-1} s_h^2 + \frac{1}{6} \gamma_{i,h} s_h^3 \right) \\ \qquad \qquad \qquad = \theta_{i,4} \\ G^0 \text{ continuity: } \begin{cases} x_{\text{traj}}(s_0) + \int_0^{s_4} \cos(\theta_1(s))\cos(\theta_2(s))ds = x_{\text{traj}}(s_e) \\ y_{\text{traj}}(s_0) + \int_0^{s_4} \cos(\theta_1(s))\sin(\theta_2(s))ds = y_{\text{traj}}(s_e) \\ z_{\text{traj}}(s_0) + \int_0^{s_4} \sin(\theta_1(s))ds = z_{\text{traj}}(s_e) \end{cases} \end{array} \right\} \quad i = 1, 2 \quad (44)$$

It can be seen from Eq. (44) that totally 9 equations and 12 unknown variables ( $\gamma_{i,j}$ ,  $s_j(i = 1, 2; j = 1, 2, 3, 4)$ ) are obtained. To solve these equations, 3 redundant variables should be fixed. In this article, we fix that  $s_1 = s_2 = s_3 = s_4$  to avoid the solutions where one or more of  $s_j < 0$  ( $j = 1, 2, 3, 4$ ). The first six equations ( $G^3$ ,  $G^2$  and  $G^1$  continuity) can be analytically solved as follows.

$$\left. \begin{array}{l} \gamma_{i,2} = \frac{3\Delta\theta_i - 3(\Delta\kappa_i + 4\kappa_{i,0})s_1 + (\Delta c_i - 12c_{i,0})s_1^2}{3s_1^3} - 3\gamma_{i,1} \\ \gamma_{i,3} = \frac{2\Delta\kappa_i - (\Delta c_i + 8c_{i,0})s_1}{2s_1^2} - 3\gamma_{i,1} - 2\gamma_{i,2} \\ \gamma_{i,4} = \frac{\Delta c_i}{s_1} - \gamma_{i,1} - \gamma_{i,2} - \gamma_{i,3} \end{array} \right. \quad (45)$$

where  $\Delta\theta_i = \theta_{i,4} - \theta_{i,0}$ ,  $\Delta\kappa_i = \kappa_{i,4} - \kappa_{i,0}$  and  $\Delta c_i = c_{i,4} - c_{i,0}$  ( $i = 1, 2$ ). Because the last three equations in Eq. (44) include Fresnel integrals, they cannot be analytically solved. The Powell dogleg method [42] is adopted to numerically solve the last three equations with unknown variables being  $\gamma_{1,1}$ ,  $\gamma_{2,1}$  and  $s_1$ .

It should be pointed out that the above fitting algorithm is also valid for 2D case. In this case, because  $\theta_{1,j-1} = \kappa_{1,j-1} = c_{1,j-1} = \gamma_{1,j} = 0$  ( $j = 1, 2, 3, 4$ ), Eq. (44) is reduced to

$$\begin{cases} G^3 \text{ continuity: } c_{2,0} + \sum_{h=1}^4 \gamma_{2,h} s_h = c_{2,4} \\ G^2 \text{ continuity: } \kappa_{2,0} + \sum_{h=1}^4 \left( c_{2,h-1} s_h + \frac{1}{2} \gamma_{2,h} s_h^2 \right) = \kappa_{2,4} \\ G^1 \text{ continuity: } \theta_{2,0} + \sum_{h=1}^4 \left( \kappa_{2,h-1} s_h + \frac{1}{2} c_{2,h-1} s_h^2 + \frac{1}{6} \gamma_{2,h} s_h^3 \right) = \theta_{2,4} \\ G^0 \text{ continuity: } \begin{cases} x_{\text{traj}}(s_0) + \int_0^{\bar{s}_4} \cos(\theta_2(s)) ds = x_{\text{traj}}(s_e) \\ y_{\text{traj}}(s_0) + \int_0^{\bar{s}_4} \sin(\theta_2(s)) ds = y_{\text{traj}}(s_e) \end{cases} \end{cases} \quad (46)$$

By fixing that  $s_1 = s_2 = s_3 = s_4$ , totally we have 5 equations (Eq. (46)) and 5 variables ( $\gamma_{2,j}$  ( $j = 1, 2, 3, 4$ ) and  $s_1$ ). Similarly, the first three equations in Eq. (46) can be analytically solved by Eq. (45) with  $i = 1$ , and the last two equations can be numerically solved with Powell dogleg method [42] with the unknown variables being  $\gamma_{2,1}$  and  $s_1$ .

Based on the solved variables  $\gamma_{i,j}$  and  $s_j$  ( $i = 1, 2; j = 1, 2, 3, 4$ ), the general clothoid spline can be fully determined with Eqs. (17)-(23). Finally, the clothoid spline is inversely transformed to the Cartesian coordinate system, as shown in Fig. 6.

$$\tilde{\mathbf{P}}(s) = \mathbf{T}^{-1}\mathbf{P}(s) = \mathbf{T}^T\mathbf{P}(s) \quad (47)$$

The corner smoothing of 3D G01/G02/G03 commands with  $G^3$  continuity is realized. Some typical examples are shown in Fig. 7. It can be seen that the proposed corner smoothing algorithm shows good smoothing performance in all the cases, i.e. the planar pairs of line-line, line-arc and arc-arc, and the space pairs of line-line, line-arc and arc-arc.

### 3.2. Constraining of the fitting error

In this section, the smoothing error is constrained within the tolerance. The smoothing error  $e$  is defined as the maximum distance from the original trajectory to the clothoid spline.

$$e = \max_{s_0 \leq \hat{s} \leq s_e} \left\{ \min_{0 \leq \bar{s} \leq \bar{s}_4} \| \mathbf{P}_{\text{traj}}(\hat{s}) - \mathbf{P}(\bar{s}) \|_2 \right\} \quad (48)$$

For the symmetrical cases, i.e. the line-line pairs and arc-arc pairs with the two segments of trajectory being symmetrical about a plane, as shown in Figs. 7(a), (b), (c), (f) and (g). The smoothing error can be analytically calculated as the distance between the corner point and the middle point of the clothoid spline.

$$e = \| \mathbf{P}_{\text{traj}}(s_c) - \mathbf{P}(\bar{s}_2) \|_2 \quad (49)$$

However, for the general line-arc pairs and arc-arc pairs (Figs. 7(d), (e) and (h)-(i)), there is no analytical expression of the fitting error. Therefore, the fitting error needs to be numerically constrained within the tolerance. The algorithms that constrain the smoothing error are developed with the following three steps, and are given in Algorithms 1, 2 and 3.

- Step 1: Compute the distance between a certain point on the trajectory and the clothoid spline (Algorithm 1).
- Step 2: Compute the maximum distance between the trajectory and the clothoid spline (Algorithm 2).
- Step 3: Limit the maximum distance to the given tolerance (Algorithm 3).

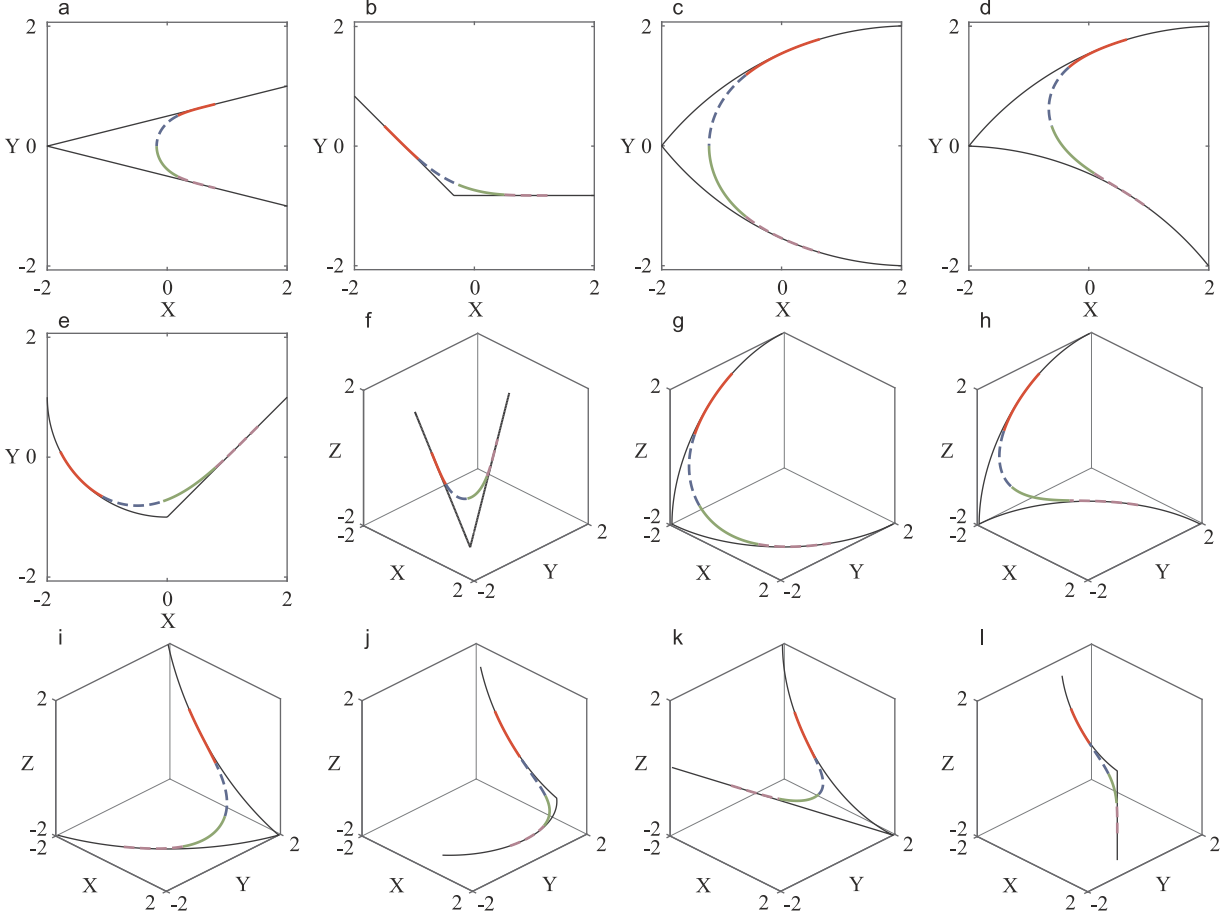


Fig. 7. Fitting examples of the proposed method.

#### 4. Simulation and experimental verification

This section presents the simulation and experimental verification of the proposed corner smoothing algorithm. To provide a comprehensive illustration of the proposed algorithm, three different cases are studied, i.e. the trajectories containing space corners, the trajectories containing planar corners with G02/G03 commands, and the trajectories containing planar corners with only G01 commands. The experiments are conducted on an in-house developed open-architecture CNC machine tool after geometric error compensation [43], as shown in Fig. 8. The sampling frequency is set as 1kHz. The commonly used P-PI controller is used to control the servo axes, and the diagram is shown in Fig. 9.

##### 4.1. Case 1: Space corners

The bowl-shape trajectory shown in Fig. 2 is used to illustrate the performance of the proposed corner smoothing algorithm for trajectories containing space corners. The smoothing error tolerance is set as 100  $\mu\text{m}$ . The trajectory after corner smoothing with the proposed method is shown in Fig. 10. Because the deviation is small, the trajectories before and after smoothing almost coincide with each other. Several typical corners are enlarged to show the performance of the corner smoothing. It can be seen that the general clothoid splines connect the space corners smoothly. Also, the curvature and sharpness of three typical corners are shown in Fig. 11. The curvature is smooth and the sharpness, which is the derivative of curvature with respect to curve length, is continuous. These validate that the proposed algorithm achieves the corner smoothing of space corners with  $G^3$  continuity.

The maximum errors between the original trajectory and the smoothed trajectory at each corner are shown in Fig. 12. It can be seen that the smoothing errors are well constrained within the tolerance. This proves the effectiveness of the algorithms that constrain the fitting error in Section 3.2.

Next, the proposed method is compared with two existing methods, i.e. the method without smoothing and the smoothing method with the traditional quintic B-splines, to show its advantage in increasing machining efficiency. Because the quintic B-spline method can only be applied to the line to line transitions, and thus, the bowl-shape trajectory has to be converted to a series of line segments. The approximation method given in Ref. [44] is adopted to subdivide the trajectory. To constrain the approximation error within the tolerance (100  $\mu\text{m}$ ), the bowl-shape trajectory is discretized to 128 small line segments. The G01 bowl-shape trajectory is then smoothed with quintic B-splines. All the trajectories, which are not smoothed, smoothed by the proposed general clothoid spline, and smoothed by the quintic B-spline method, are planned with cubic-acceleration profile proposed by Erkorkmaz [45].

The feedrate profiles are planned with the maximum feedrate of 50 mm/s, the maximum acceleration of 400 mm/s<sup>2</sup> and the maximum jerk of 5000 mm/s<sup>3</sup>. The feedrate profiles of all the trajectories after planning are shown in Fig. 13. It can be seen that under the same constraint, the machining time of the proposed method is much lower than those of the B-spline method and the point-to-point method. The machining time of the bowl-shape trajectory smoothed with the proposed method is 10.41 s, which is reduced by 14.11% and 30.7% compared with the point-to-point method (12.12 s) and B-spline method (15.02 s).

For the trajectories without smoothing, a full-stop is required at the corners. However, after smoothing with the proposed general clothoid spline, the feedrate does not need to reduce to 0 at the corners. This can increase the machining efficiency. Because the traditional B-spline method cannot directly smooth the arcs, the bowl-shape trajectory needs to be subdivided to a series of line-segments. After subdividing, the curve length of each segment is too small to accelerate to the maximum feedrate. As a result, the machining time of the trajectory

**Input:** Curve length parameter of a point on trajectory  $s_{\text{traj}}$ , the trajectory  $\mathbf{P}_{\text{traj}}(s)$ , the clothoid spline  $\mathbf{P}(s)$

**Output:** Distance  $d$  between the point and the clothoid spline

```

1  $\varepsilon \leftarrow 1 \times 10^{-7}$ 
2  $s_{\text{clo},1} \leftarrow \frac{s_{\text{traj}} - s_0}{s_e - s_0} \tilde{s}_4$ 
3 repeat
4    $s_{\text{clo},0} \leftarrow s_{\text{clo},1}$ 
5    $f_0 \leftarrow \mathbf{P}'(s_{\text{clo},0})^T (\mathbf{P}(s_{\text{clo},0}) - \mathbf{P}_{\text{traj}}(s_{\text{traj}}))$ 
6    $df_0 \leftarrow \mathbf{P}''(s_{\text{clo},0})^T (\mathbf{P}(s_{\text{clo},0}) - \mathbf{P}_{\text{traj}}(s_{\text{traj}})) + 1$ 
7    $s_{\text{clo},1} \leftarrow s_{\text{clo},0} - \frac{f_0}{df_0}$ 
8 until  $|s_{\text{clo},1} - s_{\text{clo},0}| < \varepsilon$ 
9  $d \leftarrow \|\mathbf{P}(s_{\text{clo},1}) - \mathbf{P}_{\text{traj}}(s_{\text{traj}})\|$ 

```

Algorithm 1. Distance\_PointToClothoid

---

**Input:** The clothoid spline  $\mathbf{P}(s)$ , the trajectory  $\mathbf{P}_{\text{traj}}(s)$   
**Output:** The maximum distance  $e$  between the trajectory and the clothoid spline

```

1  $\varepsilon \leftarrow 1 \times 10^{-6}$ 
2  $r_b \leftarrow 0.4$ 
3  $s_{\text{traj},l} \leftarrow s_0; g_l \leftarrow 0$ 
4  $s_{\text{traj},r} \leftarrow s_e; g_r \leftarrow 0$ 
5  $s_{\text{traj},m} \leftarrow (1 - r_b)s_{\text{traj},l} + r_b s_{\text{traj},r}$ 
6  $g_m \leftarrow -\text{Distance\_PointToClothoid}(s_{\text{traj},m}, \mathbf{P}_{\text{traj}}, \mathbf{P})^2$ 
7 while true do
8    $\alpha_1 \leftarrow \frac{g(s_{\text{traj},l}) - g(s_{\text{traj},r})}{s_{\text{traj},l} - s_{\text{traj},r}}$ 
9    $\alpha_2 \leftarrow \frac{s_{\text{traj},l} - s_{\text{traj},m}}{s_{\text{traj},m} - s_{\text{traj},r}} - \alpha_1$ 
10   $\bar{s}_{\text{traj}} \leftarrow \frac{1}{2}(s_{\text{traj},l} + s_{\text{traj},r} - \frac{\alpha_1}{\alpha_2})$ 
11   $\bar{g} \leftarrow -\text{Distance\_PointToClothoid}(\bar{s}_{\text{traj}}, \mathbf{P}_{\text{traj}}, \mathbf{P})^2$ 
12  if  $|\bar{g} - g_m| < \varepsilon$  then
13     $e \leftarrow \sqrt{-\bar{g}}$ 
14    break
15  end
16  if  $\bar{s}_{\text{traj}} < s_{\text{traj},m}$  then
17    if  $\bar{g} < g_m$  then
18       $s_{\text{traj},l} \leftarrow \bar{s}_{\text{traj}}, g_l \leftarrow g_m$ 
19       $s_{\text{traj},m} \leftarrow \bar{s}_{\text{traj}}, g_m \leftarrow \bar{g}$ 
20    else
21       $s_{\text{traj},l} \leftarrow \bar{s}_{\text{traj}}, g_l \leftarrow \bar{g}$ 
22    end
23  else
24    if  $\bar{g} < g_m$  then
25       $s_{\text{traj},l} \leftarrow s_{\text{traj},m}, g_l \leftarrow g_m$ 
26       $s_{\text{traj},m} \leftarrow \bar{s}_{\text{traj}}, g_m \leftarrow \bar{g}$ 
27    else
28       $s_{\text{traj},r} \leftarrow \bar{s}_{\text{traj}}, g_r \leftarrow \bar{g}$ 
29    end
30  end
31 end
```

---

Algorithm 2. Distance\_TrajectoryToClothoid

---

**Input:** The trajectory  $\mathbf{P}_{\text{traj}}(s)$ , the fitting error limit  $e_{\lim}$

**Output:** The clothoid spline  $\mathbf{P}(s)$  that follow the fitting error limit

```

1    $\varepsilon \leftarrow 1 \times 10^{-5}$ 
2    $s_{0,0} \leftarrow s_c, s_{e,0} \leftarrow s_c$ 
3    $h_0 \leftarrow e_{\lim}$ 
4    $s_{0,1} \leftarrow s_c - \min(0.5\text{Length}(\mathbf{P}_{\text{traj},1}), 0.5\text{Length}(\mathbf{P}_{\text{traj},2}))$  /*Length( $\mathbf{P}_{\text{traj},k}$ )( $k = 1, 2$ ) means the curve length of the  $k$ th segment*/
5    $s_{e,1} \leftarrow 2s_c - s_{0,1}$ 
6   Construct general clothoid spline  $\mathbf{P}(s)$  based on the method in Section 3 with the start and end point parameters being  $s_{0,1}$  and  $s_{e,1}$ 
7    $h_1 \leftarrow e_{\lim} - \text{Distance\_TrajectoryToClothoid}(\mathbf{P}(s), \mathbf{P}_{\text{traj}}(s))$ 
8   if  $h_1 > 0$  then
9     return  $\mathbf{P}(s)$ 
10  end
11  repeat
12     $s_{0,2} \leftarrow s_{0,1} - \frac{s_{0,1}-s_{0,0}}{h_1-h_0}h_1$ 
13     $s_{e,2} \leftarrow 2s_c - s_{0,2}$ 
14    Construct general clothoid spline  $\mathbf{P}(s)$  based on the method in Section 3 with the start and end point parameters being  $s_{0,2}$  and  $s_{e,2}$ 
15     $h_2 \leftarrow e_{\lim} - \text{Distance\_TrajectoryToClothoid}(\mathbf{P}(s), \mathbf{P}_{\text{traj}}(s))$ 
16     $s_{0,0} \leftarrow s_{0,1}, s_{e,0} \leftarrow s_{e,1}, h_0 \leftarrow h_1$ 
17     $s_{0,1} \leftarrow s_{0,2}, s_{e,1} \leftarrow s_{e,2}, h_1 \leftarrow h_2$ 
18  until  $|h_2| < \varepsilon$ 

```

---

Algorithm 3. ConstraintFittingError

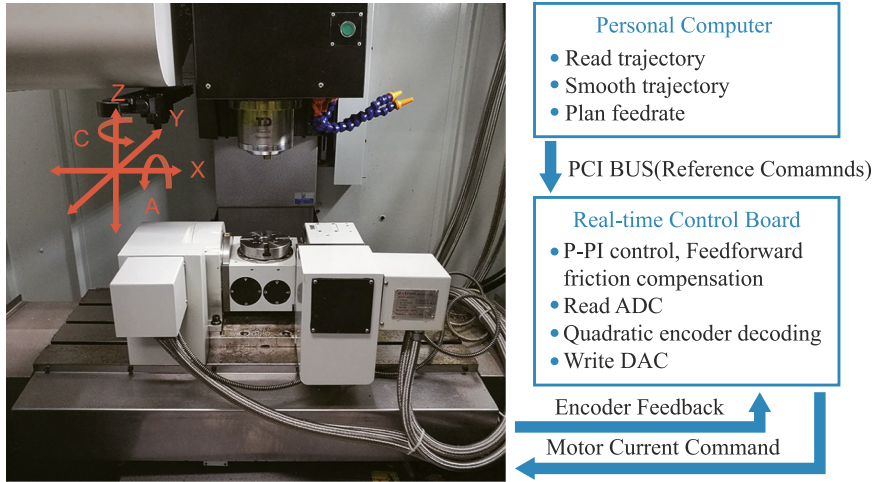


Fig. 8. The in-house developed open-architecture CNC machine tool.

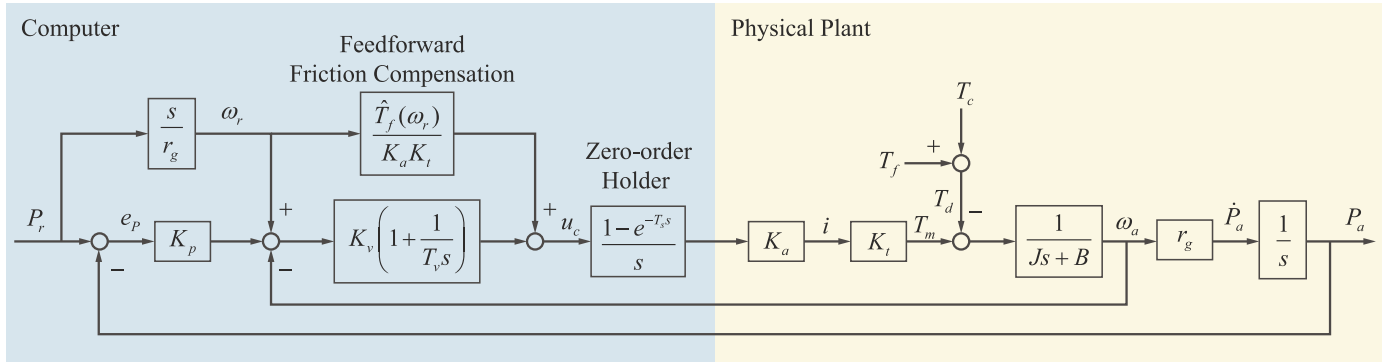


Fig. 9. The block diagram of each servo axis in experiments.

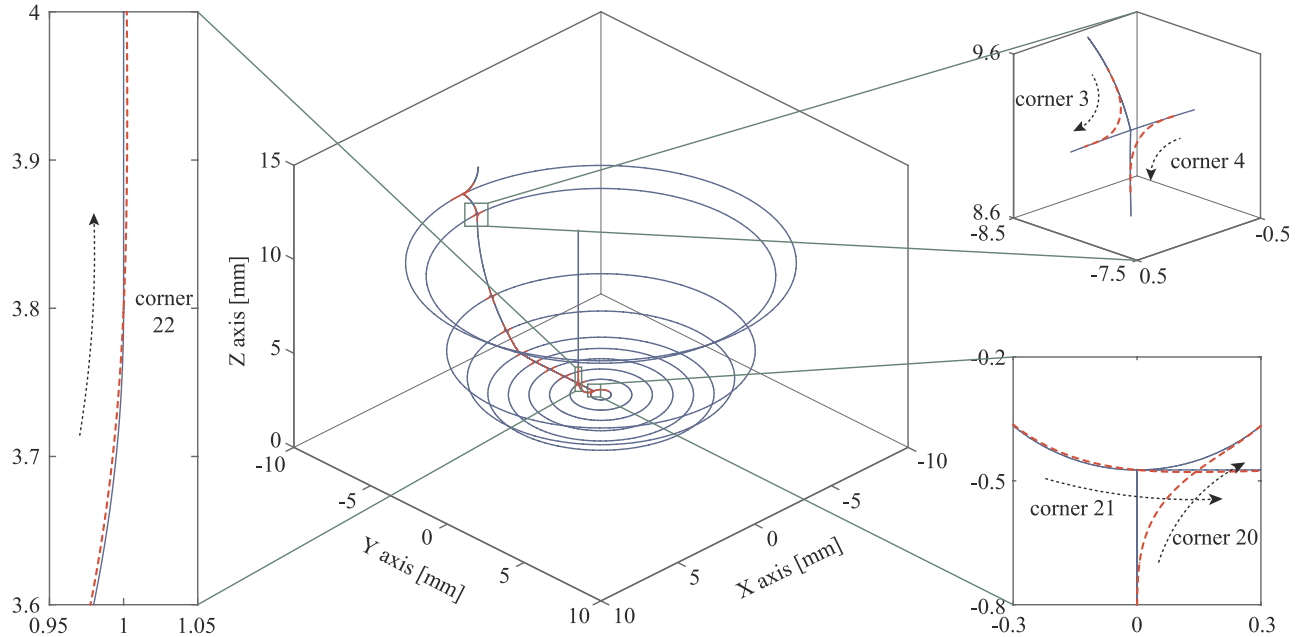
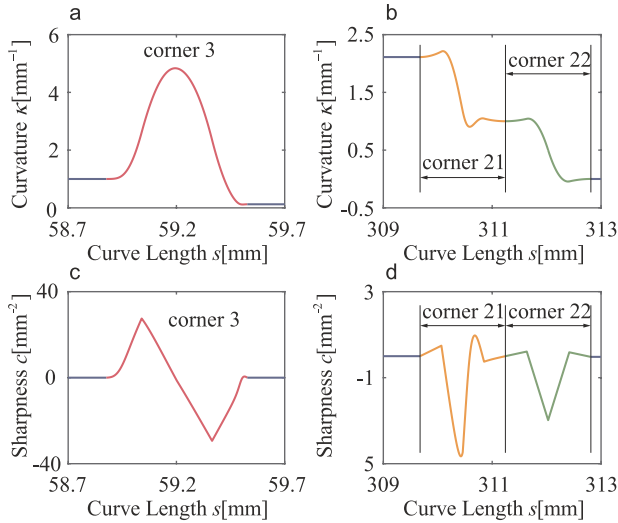
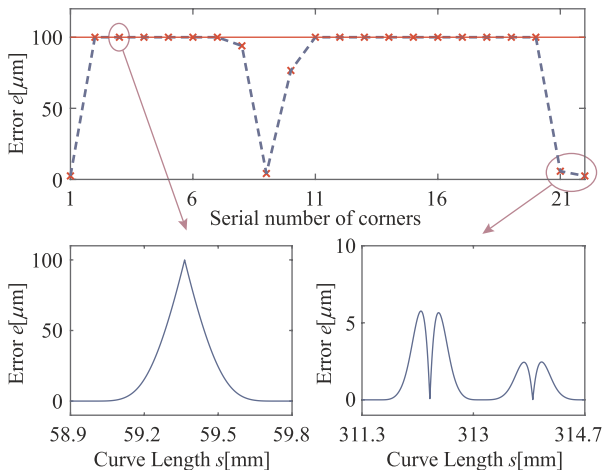


Fig. 10. The bowl-shape trajectory after smoothing with the proposed method.



**Fig. 11.** The curvature and sharpness of three typical corners of the bowl-shape trajectory after smoothing with the proposed method.



**Fig. 12.** The fitting errors of the bowl-shape trajectory after smoothing with the proposed method.

smoothed by B-spline is even longer than that of the trajectory without smoothing. By contrast, the proposed method can directly smooth the 3D arcs. Without subdividing, each arc is long enough to accelerate to the maximum feedrate. Therefore, the proposed method is able to improve the machining efficiency.

#### 4.2. Case 2: Planar corners with G02/G03 commands

In this section, the trajectories containing planar corners with G02/G03 commands are used to exam the performance of the proposed method. A flower-shape trajectory, as shown in Fig. 14(a), is taken as an example of the experiment.

The flower-shape trajectory is composed of a series of arcs. It may seem to be smooth. However, because the curvature is discontinuous at the junction of arcs, the flower-shape trajectory is  $G^2$  discontinuous. Just because of that, the acceleration of each axis will change abruptly at the junction of arcs, which will cause large tracking error. This phenomenon is shown in Fig. 15. During the experiment, both the original and the smoothed trajectories are planned with a constant

feedrate of 50 mm/s. The air-cutting experiments are conducted on the in-house developed open-architecture CNC machine tool (Fig. 8). For the flower-shape trajectory without smoothing, it can be seen from Fig. 15 that the tracking error has peaks at the curvature discontinuous points, which will greatly deteriorate the machining precision and surface integrity of machined parts. While for the smoothed trajectory with the proposed method, the tracking error is uniform without peaks.

Compared with  $G^2$  methods, which blend the arcs with traditional clothoid, the proposed method can assure the  $G^3$  continuity of the smoothed trajectory. After planning with jerk continuous feedrate profile [45], the jerk commands of the trajectory smoothed with the proposed method will be continuous. However, if smoothed with traditional clothoid, the trajectory will be  $G^3$  discontinuous. Even if planned with jerk continuous feedrate profile, the jerk commands of the flower-shape trajectory will be discontinuous. Theoretically, the jerk is infinite at the  $G^3$  discontinuous points. In practice, the jerk will not be infinite because of the limited driving capability. Still, the jerk will be large and will cause vibration of the machine tool, as can be seen in Figs. 16 and 17.

Both flower trajectories smoothed by the proposed method and by the traditional clothoid are first planned with the jerk continuous feedrate profile [45] and then used to control the machine tool. It can be seen from Fig. 16 that the actual jerk of the worktable with the traditional clothoid is much larger than that with the proposed method, no matter X axis or Y axis is concerned. At the same time, the actual acceleration of the worktable is measured by attaching an accelerometer to the table. It can be seen from Fig. 17 that the acceleration of the proposed method is much lower than that of the traditional clothoid in high frequency range. Around 160Hz, the amplitude of acceleration is reduced by 47.9% for X axis (from  $37.68 \text{ mm/s}^2$  to  $19.64 \text{ mm/s}^2$ ), and is reduced by 38.9% for Y axis (from  $34.14 \text{ mm/s}^2$  to  $20.85 \text{ mm/s}^2$ ).

Finally, cutting experiments are carried out on a three-axis CNC machine tool. The smoothed and original trajectories are machined by a ball-end cutter with the diameter being 2 mm. A constant feed-rate of 50 mm/s is adopted except the acceleration/deceleration phase. The machining results are shown in Fig. 18. It can be seen that vibration induced by the curvature discontinuity leaves marks on the original flower trajectory, as shown in Fig. 18(a). Therefore, the surface is rough and the surface quality is greatly degraded. However, as can be seen from Fig. 18(b), the surface quality of the smoothed trajectory is much better since the corner smoothing method guarantees continuous curvature and sharpness. It should be noted that one side of the trajectory is up milling and the other side is down milling. The surface qualities of the smoothed trajectory for both processing methods are better than those of the original trajectory, as can be seen in Fig. 18. Thus, the effectiveness of the proposed method is verified.

In conclusion, for trajectories containing planar corners with G02/G03 commands, the smoothing is necessary even if the trajectories seem to be smooth. Through smoothing, the proposed method can reduce the tracking errors at the curvature discontinuous points. Because the proposed method can achieve  $G^3$  continuity, the jerk and vibration of the machine tool are reduced compared with the traditional  $G^2$  methods.

#### 4.3. Case 3: Planar corners with only G01 commands

In this section, the trajectory containing planar corners with only G01 commands is used to exam the performance of the proposed method. A simple corner composed of two line segments making a  $60^\circ$  angle at their intersection is considered. The quintic B-spline method is used for comparison because both the quintic B-spline method and the method proposed in this article are  $G^3$  continuous methods. The

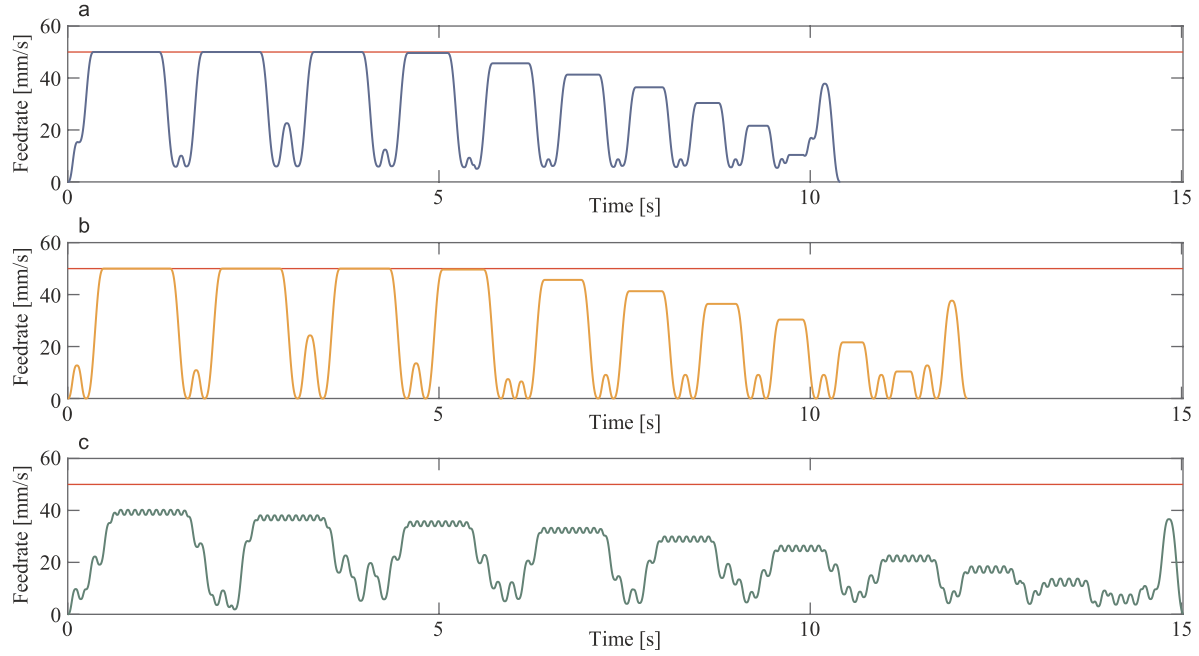


**Fig. 13.** The feedrate profiles of the bowl-shape trajectories smoothed with the proposed method (a), without smoothing (b) and smoothed with the quintic B-spline method (c).

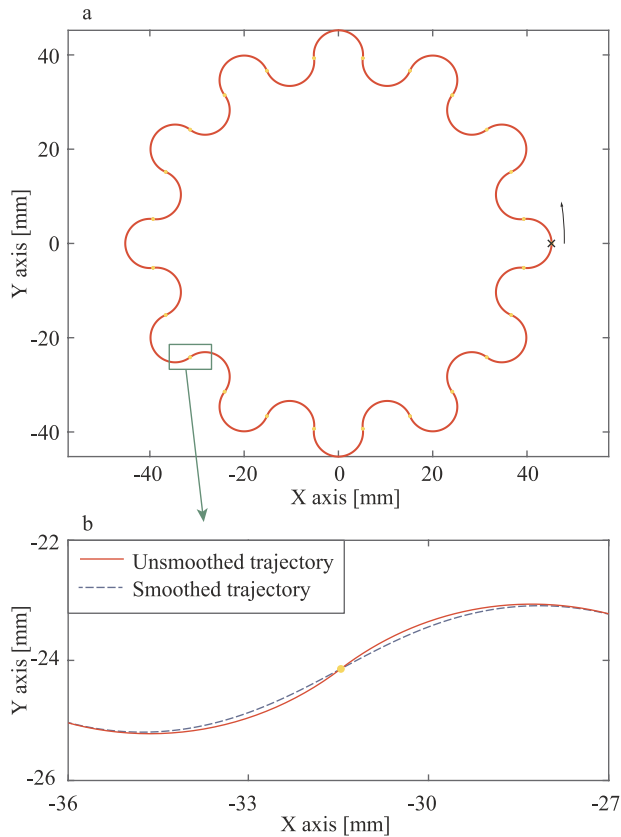


**Fig. 14.** The flower-shape trajectory (a) and its smoothing result (b) with the proposed method.

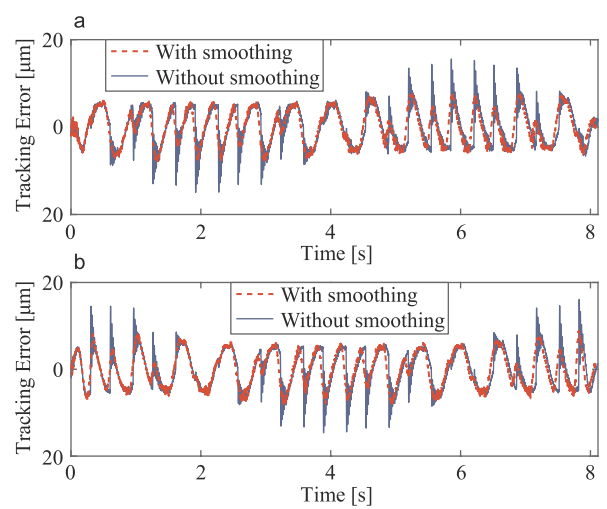


**Fig. 15.** The tracking errors of X axis (a) and Y axis (b) of the flower-shape trajectories smoothed with the proposed method and without smoothing.

smoothing results are shown in Fig. 19, where both methods are set to a smoothing tolerance of  $100 \mu\text{m}$ . It can be seen that the length of line segments required to smooth with the proposed method is less than that with the B-spline method. The curvature and sharpness of the B-spline fillets and the general clothoid spline fillets are shown in Fig. 20. It can be seen that the general clothoid spline has better curvature and sharpness profiles. Both the maximum curvature and maximum sharpness of the proposed method are smaller than those of the B-spline. The maximum curvature of the proposed method is reduced by 34.6% (from  $18.00 \text{ mm}^{-1}$  to  $11.78 \text{ mm}^{-1}$ ) and the maximum sharpness is reduced by 51.5% (from  $273.5 \text{ mm}^{-2}$  to  $132.6 \text{ mm}^{-2}$ ) compared with those of the B-spline method. It means that higher feedrate can be achieved at the corners.

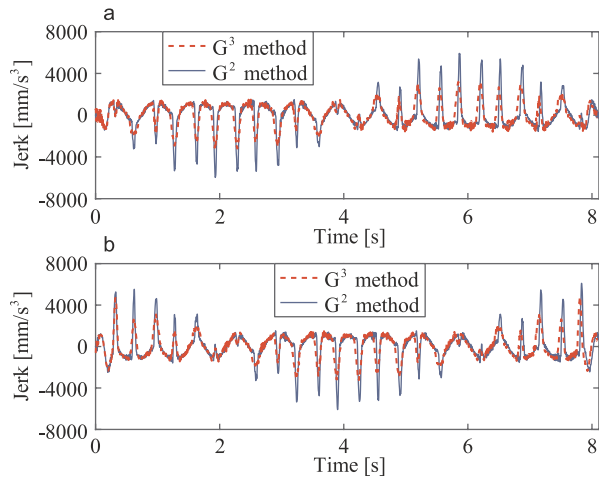


**Fig. 16.** The jerk of X axis (a) and Y axis (b) of the flower-shape trajectories smoothed with the proposed  $G^3$  method and the traditional  $G^2$  method.

## 5. Conclusions

Smoothing the trajectories before machining is critical to reduce the vibration, improve the surface finish and increase the machining efficiency. Traditional strategies are limited to the smoothing of corners in plane because of the inherent problems of curve fillets. This article establishes a new trajectory smoothing algorithm for 3-axis CNC machine tools. The traditional 2-dimensional clothoid is extended to 3-dimensional curve to accomplish the blending of space corners. The order of the traditional clothoid is increased to realize higher degree of continuity. The four-segment clothoid splines are inserted into the adjacent trajectory segments. Both mathematical derivation and simulation results indicate that the tangent, curvature and sharpness are continuous throughout the smoothed trajectory. Meanwhile, the maximum deviations between the smoothed trajectories and the original trajectories are precisely constrained within the tolerance.

Simulation and experiment results demonstrate that the machining time can be reduced by 14% after smoothing with the proposed

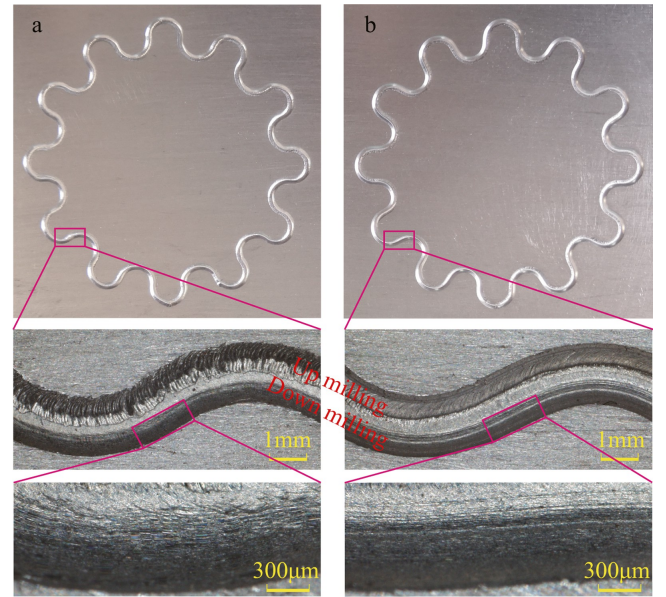


**Fig. 18.** Machining surfaces of the original (a) and the smoothed (b) flower-shape trajectory.

algorithm. Because the developed method can achieve higher degree of continuity compared to the traditional method, the trajectories are more smooth after adopting the developed smoothing method. Therefore, the amplitudes of both the acceleration in high frequency range and the jerk are reduced for each axis during the experiment. The maximum amplitude of acceleration in high frequency range is reduced by more than 38%, and the maximum jerk is reduced by more than 21%. At the same time, because the proposed 3D general clothoid has a linear sharpness profile when smoothing corners composed of line segments, the developed method can realize smaller curvature and sharpness extrema compared to those of the traditional B-spline method. It means that higher feedrate can be reached around the corner. Therefore, the machining efficiency can be increased.

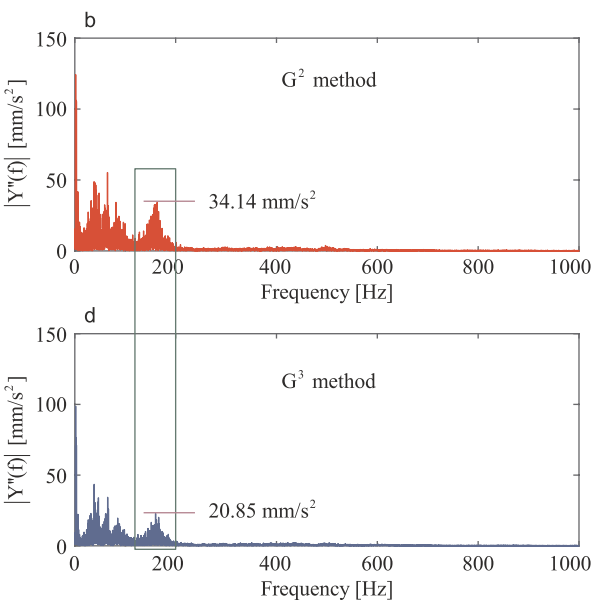
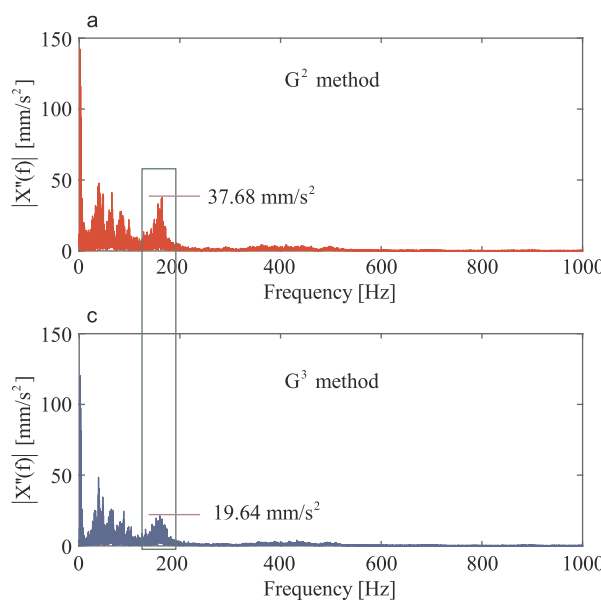


**Fig. 17.** The Fourier transformation of the acceleration of X axis (a) and Y axis (b) smoothed with the traditional  $G^2$  method and X axis (c) and Y axis (d) smoothed with the proposed  $G^3$  method.

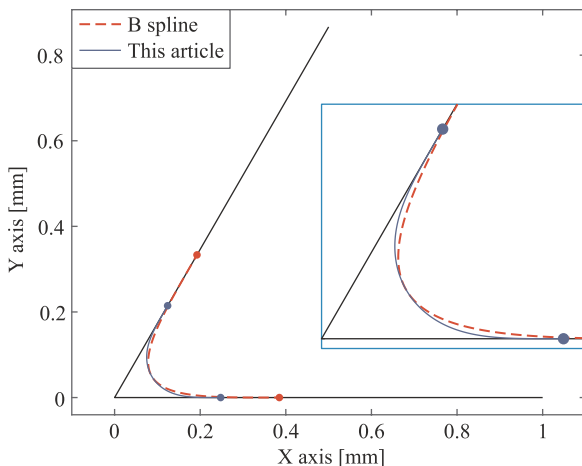


**Fig. 19.** The smoothing results of a simple corner with the proposed method and with the traditional quintic B-spline method.

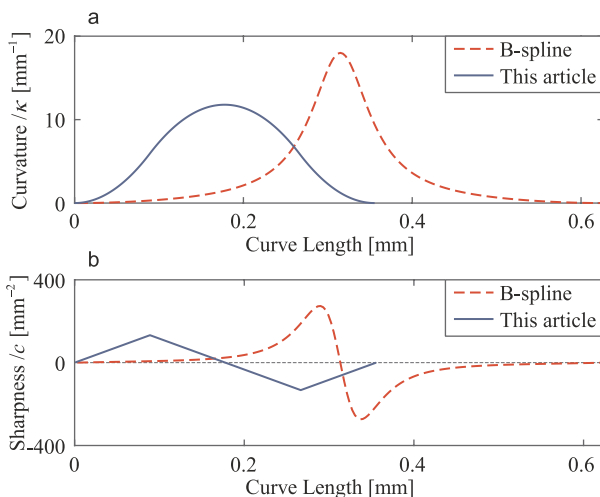


**Fig. 20.** The curvature (a) and sharpness (b) of the proposed general clothoid spline fillet and the B-spline fillet for the simple corner.

#### CRediT authorship contribution statement

**Qun-Bao Xiao:** Conceptualization, Investigation, Methodology, Software, Validation, Data curation, Visualization, Writing - original draft. **Min Wan:** Investigation, Methodology, Resources, Supervision, Writing - review & editing, Funding acquisition. **Yang Liu:** Investigation, Validation, Resources, Data curation. **Xue-Bin Qin:** Formal analysis, Investigation, Validation, Data curation. **Wei-Hong Zhang:** Project administration, Investigation, Methodology.

#### Declaration of Competing Interest

The authors declare no competing financial interests, and they have no conflicts of interest to this work.

#### Acknowledgments

This research has been supported by the National Natural Science Foundation of China under Grant nos. 51975481 and 51675440, the National Key Research and Development Program of China under Grant no. 2017YFB1102800, and the Fundamental Research Funds for the Central Universities under Grant no. 3102018gxc025.

#### References

- [1] S. Wojciechowski, M. Matuszak, B. Powalka, M. Madajewski, R. Maruda, G. Królczyk, Prediction of cutting forces during micro end milling considering chip thickness accumulation, *Int. J. Mach. Tools Manuf.* 147 (2019) 103466.
- [2] H. Wang, P. Lü, X. Cai, B. Zhai, J. Zhao, B. Wei, Rapid solidification kinetics and mechanical property characteristics of Ni-Zr eutectic alloys processed under electromagnetic levitation state, *Materials Science and Engineering: A* 772 (2020) 138660. doi: 10.1016/j.msea.2019.138660.
- [3] H. Yuan, M. Wan, Y. Yang, Design of a tunable mass damper for mitigating vibrations in milling of cylindrical parts, *Chin. J. Aeronaut.* 32 (3) (2019) 748–758.
- [4] S. Ashworth, J.P.A. Fairclough, Y. Takikawa, R. Scaife, H. Ghadbeigi, K. Kerrigan, J. Meredith, Effects of machine stiffness and cutting tool design on the surface quality and flexural strength of edge trimmed carbon fibre reinforced polymers, *Compos. Part A* 119 (2019) 88–100.
- [5] M. Chen, W.-S. Zhao, X.-C. Xi, Augmented Taylor's expansion method for B-spline curve interpolation for CNC machine tools, *Int. J. Mach. Tools Manuf.* 94 (2015) 109–119.
- [6] A. Yuen, K. Zhang, Y. Altintas, Smooth trajectory generation for five-axis machine tools, *Int. J. Mach. Tools Manuf.* 71 (2013) 11–19.
- [7] Z.C. Chen, M.A. Khan, Piecewise B-Spline tool paths with the arc-length parameter and their application on high feed, accurate CNC milling of free-form profiles, *ASME J. Manuf. Sci. Eng.* 134 (2012) 31007.
- [8] J. Huang, Y. Lu, L.-M. Zhu, Real-time feedrate scheduling for five-axis machining by simultaneously planning linear and angular trajectories, *Int. J. Mach. Tools Manuf.* 135 (2018) 78–96.
- [9] A. Gasparetto, A. Lanzutti, R. Vidoni, V. Zanotto, Experimental validation and comparative analysis of optimal time-jerk algorithms for trajectory planning, *Robot. Comput. Integrated Manuf.* 28 (2012) 164–181.
- [10] H. Zhao, L. Zhu, H. Ding, A parametric interpolator with minimal feed fluctuation for CNC machine tools using arc-length compensation and feedback correction, *Int. J. Mach. Tools Manuf.* 75 (2013) 1–8.
- [11] Q. Hu, Y. Chen, J. Yang, On-line contour error estimation and control for corner smoothed five-axis tool paths, *Int. J. Mech. Sci.* (2019) 105377, <https://doi.org/10.1016/j.ijmecsci.2019.105377>.
- [12] K. Erkorkmaz, C.-H. Yeung, Y. Altintas, Virtual CNC system. Part II. High speed contouring application, *Int. J. Mach. Tools Manuf.* 46 (2006) 1124–1138.
- [13] W. Fan, C.-H. Lee, J.-H. Chen, A realtime curvature-smooth interpolation scheme and motion planning for CNC machining of short line segments, *Int. J. Mach. Tools Manuf.* 96 (2015) 27–46.
- [14] Q. Bi, J. Shi, Y. Wang, L. Zhu, H. Ding, Analytical curvature-continuous dual-Bzier corner transition for five-axis linear tool path, *Int. J. Mach. Tools Manuf.* 91 (2015) 96–108.
- [15] B. Li, H. Zhang, P. Ye, J. Wang, Trajectory smoothing method using reinforcement learning for computer numerical control machine tools, *Robot. Comput. Integrated Manuf.* 61 (2020) 101847.
- [16] H. Zhao, L. Zhu, H. Ding, A real-time look-ahead interpolation methodology with curvature-continuous B-spline transition scheme for CNC machining of short line segments, *Int. J. Mach. Tools Manuf.* 65 (2013) 88–98.
- [17] J. Yang, A. Yuen, An analytical local corner smoothing algorithm for five-axis CNC machining, *Int. J. Mach. Tools Manuf.* 123 (2017) 22–35.
- [18] B. Sencer, E. Shamot, Curvature-continuous sharp corner smoothing scheme for Cartesian motion systems, 2014 IEEE 13th International Workshop on Advanced Motion Control (AMC), IEEE, 2014, pp. 374–379.
- [19] S. He, C. Yan, Y. Deng, C.-H. Lee, X. Zhou, A tolerance constrained  $G^2$  continuous path smoothing and interpolation method for industrial SCARA robots, *Robot. Comput. Integrated Manuf.* 63 (2020) 101907.
- [20] Q. Hu, Y. Chen, X. Jin, J. Yang, A real-time  $C^3$  continuous local corner smoothing and interpolation algorithm for CNC machine tools, *ASME J. Manuf. Sci. Eng.* 141 (2019) 41004.
- [21] J. Shi, Q. Bi, L. Zhu, Y. Wang, Corner rounding of linear five-axis tool path by dual PH curves blending, *Int. J. Mach. Tools Manuf.* 88 (2015) 223–236.
- [22] K. Wu, C. Krewet, B. Kuhlenkötter, Dynamic performance of industrial robot in corner path with CNC controller, *Robot. Comput. Integrated Manuf.* 54 (2018) 156–161.
- [23] L. Biagiotti, C. Melchiorri, FIR filters for online trajectory planning with time- and frequency-domain specifications, *Control Eng. Pract.* 20 (12) (2012) 1385–1399.
- [24] S. Tajima, B. Sencer, Accurate real-time interpolation of 5-axis tool-paths with local corner smoothing, *Int. J. Mach. Tools Manuf.* 142 (2019) 1–15.
- [25] Y. Liu, M. Wan, X.-B. Qin, Q.-B. Xiao, W.-H. Zhang, FIR filter-based continuous interpolation of G01 commands with bounded axial and tangential kinematics in industrial five-axis machine tools, *Int. J. Mech. Sci.* 169 (2020) 105325.
- [26] S. Tajima, B. Sencer, Global tool-path smoothing for CNC machine tools with uninterrupted acceleration, *Int. J. Mach. Tools Manuf.* 121 (2017) 81–95.
- [27] Q. Zhang, X.-S. Gao, H.-B. Li, M.-Y. Zhao, Minimum time corner transition algorithm with confined feedrate and axial acceleration for nc machining along linear tool path, *Int. J. Adv. Manuf. Technol.* 89 (2017) 941–956.
- [28] R. Fleisig, A. Spence, A constant feed and reduced angular acceleration interpolation algorithm for multi-axis machining, *Comput. Aided Des.* 33 (2001) 1–15.
- [29] X. Shen, F. Xie, X.-J. Liu, Z. Xie, A smooth and undistorted toolpath interpolation method for 5-DoF parallel kinematic machines, *Robot. Comput. Integrated Manuf.* 57 (2019) 347–356.
- [30] X. Du, J. Huang, L.-M. Zhu, H. Ding, An error-bounded B-spline curve approximation scheme using dominant points for CNC interpolation of micro-line toolpath, *Robot. Comput. Integrated Manuf.* 64 (2020) 101930.
- [31] C.-S. Chen, S.-K. Chen, Synchronization of tool tip trajectory and attitude based on the surface characteristics of workpiece for 6-DOF robot manipulator, *Robot. Comput. Integrated Manuf.* 59 (2019) 13–27.
- [32] K. Erkorkmaz, Y. Altintas, Quintic spline interpolation with minimal feed fluctuation, *ASME J. Manuf. Sci. Eng.* 127 (2005) 339–349.
- [33] M.K. Jouaneh, Z. Wang, D.A. Dornfeld, Trajectory planning for coordinated motion of a robot and a positioning table. I. Path specification, *IEEE Trans. Robot. Autom.* 6 (6) (1990) 735–745.

- [34] M.K. Jouaneh, D.A. Dornfeld, M. Tomizuka, Trajectory planning for coordinated motion of a robot and a positioning table. II. Optimal trajectory specification, *IEEE Trans. Robot. Autom.* 6 (6) (1990) 746–759.
- [35] D.H. Shin, S. Singh, Path Generation for Robot Vehicles Using Composite Clothoid Segments, Technical Report, Carnegie Mellon University, Pittsburgh, PA, 1990. CMU-RI-TR-90-31.
- [36] M. Brezak, I. Petrović, Path smoothing using clothoids for differential drive mobile robots, *IFAC Proc. Vol.* 44 (1) (2011) 1133–1138.
- [37] A. Shahzadeh, A. Khosravi, S. Nahavandi, Path planning for CNC machines considering centripetal acceleration and jerk, *2013 IEEE International Conference on Systems, Man, and Cybernetics*, IEEE, 2013, pp. 1759–1764.
- [38] A. Shahzadeh, A. Khosravi, T. Robinette, S. Nahavandi, Smooth path planning using bi-clothoid fillets for high speed CNC machines, *Int. J. Mach. Tools Manuf.* 132 (2018) 36–49.
- [39] F. Bertails-Descoubes, Super-clothoids, *Computer Graphics Forum*, 31 Wiley Online Library, 2012, pp. 509–518.
- [40] R. Casati, F. Bertails-Descoubes, Super space clothoids, *ACM Trans. Graph.* 32 (4) (2013) 48.
- [41] G. Harary, A. Tal, 3D Euler spirals for 3D curve completion, *Proceedings of the Twenty-Sixth Annual Symposium on Computational Geometry*, ACM, 2010, pp. 393–402.
- [42] I. Sandro, V. Parisi, A FORTRAN subroutine for solving systems of nonlinear simultaneous equations, *Comput. J.* 24 (1981) 87–91.
- [43] Y. Liu, M. Wan, Q.-B. Xiao, W.-H. Zhang, Identification and compensation of geometric errors of rotary axes in five-axis machine tools through constructing equivalent rotary axis (ERA), *Int. J. Mach. Sci.* 152 (2019) 211–227.
- [44] D.J. Walton, D.S. Meek, Approximation of quadratic Bezier curves by arc splines, *J. Comput. Appl. Math.* 54 (1) (1994) 107–120.
- [45] K. Erkorkmaz, Optimal Trajectory Generation and Precision Tracking Control for Multi-Axis Machines, University of British Columbia, 2004 Ph.D. thesis.